ACS OMEGA

http://pubs.acs.org/journal/acsodf

Review

Strategies To Modify the Surface and Bulk Properties of 3D-Printed Solid Scaffolds for Tissue Engineering Applications

Ruchira Chakraborty, Abhijeet Govind Anoop, Abhay Thakur, Girish Chandra Mohanta,* and Prasoon Kumar*

Cite This: *ACS Omega* 2023, 8, 5139−5156

Read Online

ACCESS | Metrics & More | Article Recommendations

ABSTRACT: 3D printing is one of the effective scaffold fabrication techniques that emerged in the 21st century that has the potential to revolutionize the field of tissue engineering. The solid scaffolds developed by 3D printing are still one of the most sought-after approaches for developing hard-tissue regeneration and repair. However, applications of these solid scaffolds get limited due to their poor surface and bulk properties, which play a significant role in tissue integration, loadbearing, antimicrobial/antifouling properties, and others. As a result, several efforts have been directed to modify the surface and bulk of these solid scaffolds. These modifications have significantly improved the adoption of 3D-printed solid scaffolds and devices in the healthcare industry. Nevertheless, the in vivo implant applications of these 3D-printed solid scaffolds/devices are still under development. They require attention in terms of their surface/bulk properties, which dictate their functionality. Therefore, in the current review, we have discussed different 3D-printing parameters that facilitate the fabrication of solid scaffolds/devices with different properties. Further, changes in the bulk properties through material and microstructure modification are also being discussed. After that, we deliberated on the techniques that modify the surfaces through chemical and material modifications. The computational approaches for the bulk modification of these 3D-printed materials are also mentioned, focusing on tissue engineering. We have also briefly discussed the application of these solid scaffolds/devices in tissue engineering. Eventually, the review is concluded with an analysis of the choice of surface/bulk modification based on the intended application in tissue engineering.

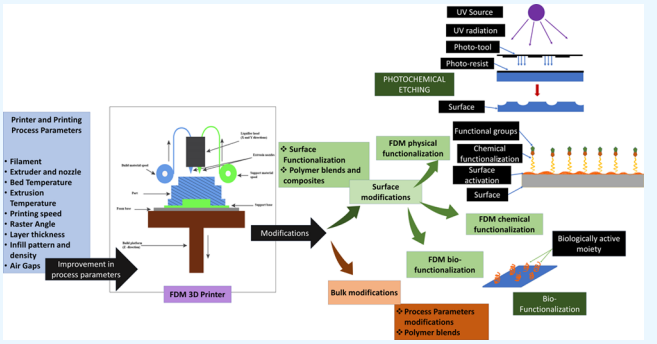

1. INTRODUCTION

3D printing is a significant manufacturing technique from automobiles to the biomedical industry.[1,2] Fused deposition modeling (FDM) is a type of 3D-printing technique that has recently gained the limelight owing to its simplistic operation, cost-friendliness, and portability. Hence, FDM has become an excellent choice for prototyping purposes. With the introduction of a plethora of materials being processed through FDM and its variants, it has also been explored in tissue engineering and regenerative medicine.[3]

The scaffolds and devices developed from FDM generally lack the mechanical and surface properties required for tissue engineering applications.[4,5] One of the most explored materials in the area, poly(lactic acid) (PLA), does not exhibit good elastic properties and, hence, faces difficulty in applications demanding flexibility/deformation. The PLA exhibits low crystallinity, low impact strength, brittleness, and low elongation at the break-even point, which precludes its usage in orthopedic and dental applications.[6] This has led to several studies where researchers have modified the FDM material by blending it with nanomaterials to create a nanocomposite.[7] For instance, Pentek et al. have FDM printed a carbon nanocomposite to develop structures with enhanced mechanical properties. It was observed that there had been enhanced mechanical properties due to adding a small number of nanomaterials.[8] Although the development of such materials enhances the mechanical strength of the FDM-printed components, the chemical properties of the developed material may get altered due to such modifications.[8] For example, Silva et al. observed that surface properties, such as hydrophilicity, get altered by blending PLA with carbon nanotubes (CNT).[9] Oxygen plasma etching incorporated multiwalled CNT increase oxidation and improve cell viability. The changes in

Received: September 15, 2022
Accepted: January 5, 2023
Published: January 30, 2023

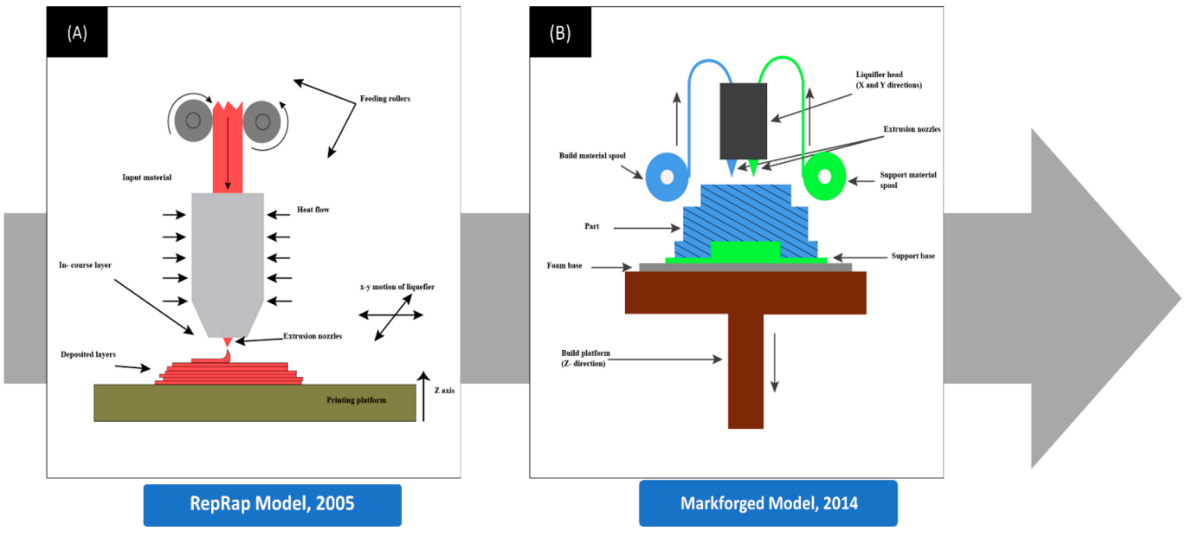

Figure 1. (A) Schematic diagram of a 3D printer during the initial stages of the RepRap project during the early 2000s. The most distinguishing difference would be the presence of just a single extruder extruding only the single input material and the absence of a support base or support structures. (B) Schematic diagram of the more advanced continuous filament fabrication 3D technology introduced by Markforged later in 2014. The 3D printer used two extrusion nozzles to extrude the filament and lay strands of reinforcing fibers that formed the backbone. (B) Components. (i) The build platform, also called the bed, is the part of the printer where the object is printed. The build platforms may be heated to prevent warping. Increasing the temperature of build platforms also reduced deformations and shrinkage. (ii) The support base is used to keep the models fixed to the build platform while printing. (iii) The extrusion nozzle squeezes out the thermoplastic material layer-wise to form the final product. The diameter of the extrusion nozzle determines the layer thickness. (iv) The increased layer thickness reduced ductility and increased failures. (v) The liquefier head is where the thermoplastic filament is melted inside to a semimolten stage.

the surface properties of a 3D-printed carbon nanocomposite significantly affect cellular behavior, especially cell adhesion, cell viability, and osteoblast differentiation.[9] Kotsilkov et al. reported that scaffolds showed better cell proliferation and spreading. However, the increased concentration of nanomaterials may induce cell toxicity.[10] Further, owing to the biodegradable nature of any scaffold used in tissue engineering, the leachate of the PLA carbon nanocomposite should be below toxic limits for any in vivo applications. Therefore, it is essential to tailor the mechanical properties of FDM-printed scaffolds without negatively affecting the surface properties.

To introduce FDM-printed scaffolds in tissue engineering, the surface topology and the chemical properties should encourage cellular interaction with the material and improve biocompatibility and the requisite mechanical stimulus. A general approach adopted to achieve this was by mimicking the natural microenvironment. To achieve better surface adhesion, cytocompatibility, hemocompatibility, cell growth, and proliferation, surface and bulk functionalization are performed. Various newer methods to induce surface modifications have been recently adopted to improve surface properties and facilitate cell culture or tissue engineering applications. For example, ε-poly-L-lysine, a polypeptide, was used to surface-modify the FDM-printed PCL/HA composite scaffolds, improving surface smoothness, water uptake, and cellular attachment and proliferation on the scaffold.[11] It also improved the antibacterial properties of the scaffolds. Gold nanoparticle deposition on an acetonitrile butadiene styrene (ABS)-printed scaffold showed better cytocompatibility, cell viability, cell proliferation, and spheroid formation. Gold nanoparticle deposition on 3D-printed scaffolds can also be beneficial for developing disease models, especially cancer models, for drug testing.[12] Nanobioceramics such as hydroxyapatite and bioglass are known for their biological properties like osteoinduction and interfacial bonding to bones. Hence, they find immense utility in bone tissue engineering as a surface-modifying agent. In the study by Fazeli et al., hydroxyapatite and bioglass were deposited on the surface of a 3D-printed polycaprolactone (PCL) scaffold, and they observed enhanced osteogenic differentiation of stem cells under in vitro conditions.[13] Carbon fiber-reinforced polyether ether ketone (PEEK) is observed to have better mechanical strength than pristine PEEK but retains biocompatibility and high cell density on the scaffold under in vitro conditions.[14] These nanocomposites, where nanoparticles and nanofibers are blended with the base polymers, are being considered to develop scaffolds/devices with improved surface properties for tissue engineering applications.

The bulk mechanical and surface properties have been primarily taken care of through material modifications by either blending or coating with different nanomaterials. However, the underlying microstructures in any FDM-printed scaffold play a vital role in defining the surface and bulk properties. It has been observed that, during the fabrication process by an FDM 3D printer, the component's microstructure is hardly controlled and tailored. Recently, some researchers have expressed that raster scanning speed and pattern, degree of fusion between the molten filaments, and effect of the cooling pattern of the molten extruded filament play a vital role in determining the bulk and surface properties of the 3D-printed scaffolds. As a result, the components/devices designed and fabricated lack the requisite mechanical properties and surface texture.[15] Moreover, conventionally, the ability to tailor mechanical properties is primarily restricted to operating parameters like infill density, which determines the material density in a fabricated component or device.[16] Further, the base material used in FDM significantly determines the final mechanical/surface properties of 3D-printed components. Hence, the authors believe that the mechanical and surface properties of FDM 3D-printed

https://doi.org/10.1021/acsomega.2c05984
ACS Omega 2023, 8, 5139−5156

scaffolds and devices have not been discussed extensively to establish the relation between the (pre, during, and post) processing parameters of 3D printing and the functional properties of scaffolds/devices.

Therefore, in the current manuscript, we have explored the possibilities of FDM printers to develop scaffolds and devices in tissue engineering. We have discussed the role of microstructure and its origin through various parameters of 3D printing during FDM. Further, we have deliberated on the role of operating parameters that affect the quality of 3D-printed scaffolds, measurement, and estimation of mechanical and surface properties. We have also extensively discussed the role of surface and bulk functionalization in encouraging cell culture. We have also discussed the application of the FDM-printed scaffolds in tissue engineering and modifications proposed to achieve these scaffolds' desirable function. Eventually, we have concluded by proposing a comparative analysis showing the modifications to alter FDM-printed scaffolds' bulk and surface properties for tissue engineering applications. This review will be helpful to biomaterials, surface engineering, additive manufacturing, and tissue engineering researchers.

2. FDM 3D PRINTERS

Fused deposition modeling (FDM)-based 3D printing uses the underlying principle of melting a raw material and using that to build new and possibly more complex shapes.[17] FDM printers employ a thermoplastic filament heated to its melting temperature to a semiliquid form. It is then extruded from a metallic nozzle and deposited on a platform in a layer-by-layer format to fabricate the required three-dimensional structure.[18] A 3D printer is embedded with several mechanisms and mechanical components to fabricate the required product. The FDM 3D printers have undergone major structural changes in the last two decades, which improved the ease and efficiency of printing (Figure 1).

The main structural components of a 3D printer (Figure 1) are briefly described below.

2.1. Filament. The filament is the primary material used to fabricate the required component. Filaments used in FDM 3D printers are generally thermoplastics with low melting temperatures, such as PLA or ABS.[19] Recently, other high-performance thermoplastics such as PEEK and polyether imide (PEI) are also being explored for their suitability for FDM printers. Due to the demand for different applications, FDM researchers have developed several composite filaments. For instance, Sciancalepore et al. proposed polybutylene adipate terephthalate (PBAT)-reinforced ZTC microparticles to develop an ecofriendly biocomposite as a filament for use in 3D printers,[20] and Ju et al. proposed a blend comprising thermoplastic starch (TPS), PLA, and PBAT as a highly renewable filament, which also had minimal brittleness.[21] A PLA blend with poly(butylene succinate) exhibited improved tensile and impact strength.[22] Another blend comprising ABS with poly(methyl methacrylate) (PMMA) improved the scratch resistance of the printed parts and their mechanical strength.[23] These examples highlight the importance of composite filaments in improving their mechanical properties.

Although mechanical properties are of enormous relevance in developing scaffolds for tissue engineering applications, the innate material of a filament also plays an important role in determining the scaffold's biocompatibility. In a study by Shilov et al., scaffolds fabricated with PLA, PEEK, and polyethylene terephthalate glycol (PETG)-like biocompatible polymers were used to culture bone marrow cells and peritoneal cells. The surface characteristics, such as roughness, an indirect effect of the printer's high nozzle diameter and layer thickness, increased the adhesion of the cells in the case of PLA. In contrast, in PEEK, finer print resolution resulted in better adhesion. However, the high cell proliferation in these scaffolds indicated and cemented their promise of wide applications in the biomedical field.[24] In another example, a scaffold was modeled using a single extruder with FDM 3D printing of PLA and biphasic calcium phosphate. The filament, though, was fragile but showed excellent cytocompatibility properties examined with Detroit 551 cells.[25] The choice of filament also depends on an FDM printer's bed. The print bed is typically made up of a glass, acrylic, or metal sheet. However, to overcome the warping effect of the printed material, the bed may have a heating element.[26] The filament choices in FDM 3D printing are limited owing to the polymer's melting temperature and the effect of overheating on the filament. Lesser deformation in a PLA structure was observed in heated print beds with high bed temperatures. Further, a reduction in warping was also observed when applying epoxy resin-based adhesive onto the printing bed.[26] It is preferred for the print-bed surface to have high adhesive strength such that the printed polymer melt can stick to the surface and form the stable base layer of the designed scaffold.

2.2. Extruder and Nozzle. The extruder is the part of the printer that moves, melts, and ejects the semiliquid thermoplastic material onto the print platform in a successive layer-wise fashion. The type of extruder used and the hot end can significantly affect the quality and style of the print. The primitive version of the extruder relied on printing the support and the actual structure with the same filament. However, Sun et al. proposed a continuous fiber extruder for 3D printers with a separate print head for hydrogel 3D printing after successfully printing the support layer.[27] Pusch et al. proposed a large-volume extruder design for printing epoxies, collagens, etc. that are suitable for large structures.[28] There have been extruders that support dual extrusion of polymers with different physio-mechanical properties.[29] The extruders have been designed to handle pellets that are much more useful in printing composites/blended polymers.[30] After the thermoplastic material is heated in the heating chamber of the extruder, it then enters the nozzle and is squeezed out to form the final product with high precision. The temperature of the nozzle is kept just a few degrees above the melting point of the polymer thermoplastic filaments.[31]

2.3. Printing Process of the FDM 3D Printer. The printing process of an FDM-employed 3D printer can be broadly divided into three main stages: (1) preprocessing, (2) production, and (3) postproduction.

2.3.1. Preprocessing. In the preprocessing stage, the scaffold's design is first drawn using CAD software such as AutoCAD, SolidWorks, Fusion 360, etc. and saved in an STL format. For irregular objects like organs/tissues, computed tomography (CT) and magnetic resonance imaging (MRI) are generally preferred to achieve high accuracy in 3D design.[32] Photogrammetry is an alternative tool for creating a 3D model of irregular objects like amputee limbs for designing prosthetics. For instance, Ismail et al. generated a 3D model of trans-radial prosthetic sockets using photogrammetry and printed the socket in PLA using an FDM printer.[33] Slicing software such as Simplify 3D and Cura divides the digital

https://doi.org/10.1021/acsomega.2c05984
ACS Omega 2023, 8, 5139−5156

model into numerous layers (slices) after considering specific parameters that significantly influence the product's mechanical properties.[32] Following the slicing procedure, a G-code file for the printer is generated as an output file with the head movement of the printer being encoded on X, Y, and Z instructions. The G-code is simply a set of commands for the printer.

Preprocessing shall also include optimizing the different process parameters such as the print orientation, print bed, extrusion head temperature, printing speed, air gaps, infill pattern, and density. These parameters play a significant role in determining the mechanical and surface properties of the printed scaffolds and shall be discussed in detail in Section 3.

2.3.2. Production. Upon completion of the preprocessing stage, the thermoplastic material is heated to a semiliquid stage and is deposited, forming a 2D layer over the print platform. The Z stage rises to a few thousandths of an inch from the extrusion tip. The extrusion head then moves in an XY gantry, laying down a material filament. Upon completion of each layer, the Z stage moves down slightly to make way for the next layer. The layer-by-layer process continues until the required 3D objects are created. The temperature to which the thermoplastic filament is heated differs among different filaments, and it is generally heated to a temperature between 150 and 300 °C.[34] The 3D printer deposits a removable material or support structure that acts as a support base before the required object is printed to keep overhangs upright.[35] Polamaplly et al. proposed using cellulose hydrogels as biodegradable support structures that dissolve quickly and promote mechanical polishing.[36] Current research focuses on various other applications of support structures in 3D printing, such as dissolvable prototype parts, breakage support, assembly labels, and many more, as proposed by Nisser et al.[37]

2.3.3. Postprocessing. Once the required product has been formed, postprocessing is carried out to improve the surface roughness. Kumbhar and Mulay proposed that postprocessing is done mainly to improve the surface finish.[38] Upon completion of the printing process, the product is taken out of the printing platform, and the support structures are removed, marking the beginning of the postprocessing process. Depending upon the solubility of the support structures, they may be removed through chemical or mechanical means. The postprocessing process is categorized into two types: chemical and mechanical. The mechanical postprocessing methods mainly include machining, abrasive, barrel finishing, and sanding to improve surface roughness. Boschetto et al. used computer numerical control (CNC) milling machines to enhance the surface roughness of the 3D-printed parts in acetonitrile butadiene styrene, nylon, polyethylene, and polypropylene.[39] The chemical methods mainly involve vapor deposition, coating, and heating. Mazlan and co-workers presented a blow-cold vapor treatment process on ABS materials to improve the surface finishing.[40]

Postprocessing of FDM has been accomplished with multiple physical and chemical processes that smoothen the surface by abrasive methods, including CNC milling and cold vapor treatment, laser beam cutting,[41] manual sanding, abrasive flow machining, hot cutter machining,[42] etc. However, most of these methods are unsuitable for the postproduction processing of scaffolds as they can damage the microstructure and hamper the surface properties of the scaffold. Physical treatment processes such as plasma treatment methods and chemical treatment methods such as solvent exposure, wet chemical etching, and covalent grafting have been successfully used in the postprocessing of FDM-printed scaffolds for tissue engineering purposes and are discussed in detail in Section 5.1.

2.4. Advancements in FDM-Printing Technology. A 3D printer produces components that constantly suffer from the staircase effect. The staircase effect compromises the mechanical properties of the fabricated parts and deems them unfit for molding applications. Singamneni et al. proposed a mathematical model for curved layer deposition to overcome the challenges. They implemented modification of the G-code to achieve a curved path for the nozzle during FDM printing. They also demonstrated by printing components with curved layer deposition and highlighted improved mechanical properties of the element compared to conventional layer deposition techniques.[43] Chakraborty et al. proposed a new algorithm for the extruder path generation to achieve better curved layer deposition and allowed for the fabrication of thin curved shells.[44] Curved interlayers were achieved by laying longer lengths of filament over a larger area per layer. After that, Allen and Trask proposed using a delta robot to achieve curved layer deposition of a fused filament. This approach led to the improved surface finish of 3D-printed components and saved time and cost of printing.[45] Furthermore, there was an improvement in the strength of the fabricated parts in the *z*-direction.[45] In 2019, Chen et al. also adjusted the nozzle axis concerning the surface normal and utilized their algorithm that involves a variable-thickness and variable-depth optimized curved path to achieve successful thin-shell printing.[46] These thin shells are particularly useful in printing scaffolds for skin.

3. PARAMETERS AFFECTING THE PRINTING PERFORMANCE

3.1. Printing Process Parameters. Several parameters affect the efficiency and have a significant impact on the properties of the scaffold. The printing-process parameters can be classified into the machine and the material. The machine parameters are those that the user must specify during generating G-code files. In contrast, the material parameters include the properties of the materials being used in filaments and the materials being extruded through the nozzle.[47] The machine parameters include the bed temperature, extrusion temperature, printing speed, raster angle, layer thickness, build orientation, infill pattern, raster width, air gaps, contour numbers, etc. The material properties, such as thermal and mechanical properties, also affect the performance of the print. Doshi et al. curated the effects of various printing parameters such as building orientation, slicing parameters such as flow rate, layer thickness, deposition speed, etc., and different temperature conditions of the machine such as extrusion temperature, environmental temperature, etc. on the mechanical properties of FDM 3D-printed parts.[48] Doshi et al., after a detailed review, claimed that, with build orientation and raster angle both at 0°, 100% infill density, and 90 mm/s print speed, the best Young's modulus and tensile strength could be achieved.[48] Similarly, Samykano et al. studied the influence of process parameters on the mechanical properties of the model and determined the significant parameters as infill percent, scaffold thickness, and raster angle with response surface methodology on FDM-printed ABS.[49] A diligent study of the ABS printed part revealed that a raster angle of 55°, layer thickness of 0.5 mm, and 80% infill percentage ensured high elastic modulus, ultimate tensile strength, and good fracture strength.[49] It was also concluded that these factors and their

https://doi.org/10.1021/acsomega.2c05984
ACS Omega 2023, 8, 5139−5156

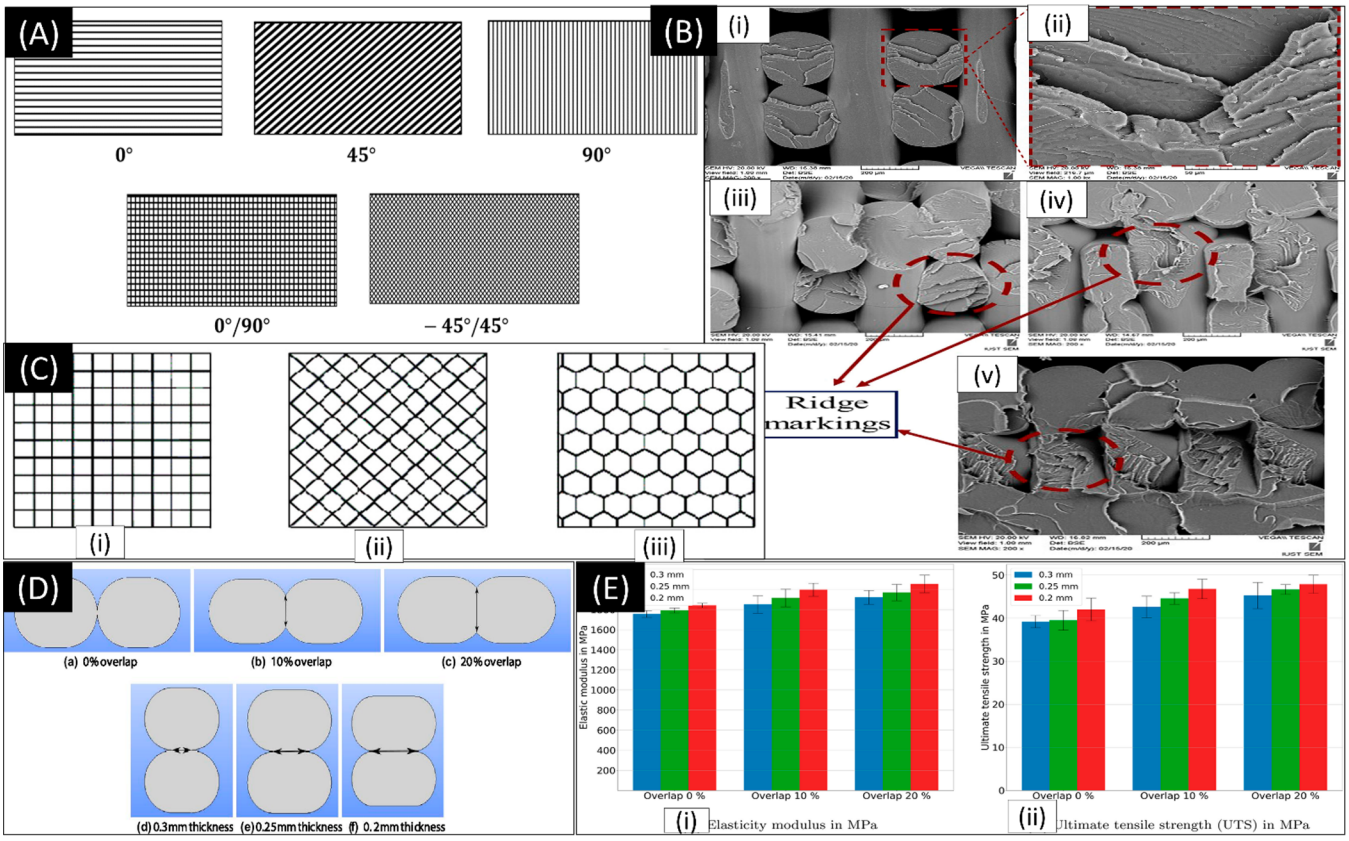

Figure 2. (A) Raster angle visualization. Reproduced with permission from ref 53 (2019), Open Access. (B) Fracture surfaces for raster angle: (i, ii) 0/90°, (iii) 15/−75°, (iv) 30/−60°, and (v) 45/−45°. Reproduced with permission from ref 62. Copyright 2020 Elsevier. (C) Infill density patterns. Reproduced with permission from ref 53 (2019), Open Access. (D, E) Overall degree and its effect on elasticity modulus and ultimate tensile strength. Reproduced with permission from ref 69 (2021), Open Access.

different combinations and interactions are significant in determining the mechanical properties.[48] Some parameters and their impact on the surface and bulk (mechanical) properties are thus individually discussed in detail in the following subsections.

3.1.1. Bed Temperature. FDM printers commonly have print beds composed of glass or polymers. The bed temperature significantly influences the adhesion of the printed material onto the print bed during printing. The print-bed temperature is commonly kept between 50 and 70 °C. However, upon a focused study on the impact of bed temperature on the mechanical properties of printed parts, Spoerk et al. observed a significant increase in adhesion forces when the bed temperature was raised slightly above the glass transition temperature of the filament.[50] Choi et al. investigated the influence of bed temperature on the shape errors of ABS parts caused by heat shrinkage. They concluded that increasing the temperature of the print bed lowered the deformed shape errors.[51] The increased temperature was also observed to improve the interlayer adhesion in FDM-printed PLA models.[54] For PLA, a printing-bed temperature between 80 and 120 °C was recommended by Spoerk et al., while for ABS, a bed temperature of at least 120 °C was recommended for proper adhesion.[52] A study conducted to determine the optimal bed temperature for ABS claimed that the deformed shape errors were minimal at higher temperatures. They also concluded from their study that 110° is the optimum because beyond 120° the laminating adhesion was not ideal.[51]

3.1.2. Extrusion Head Design and Temperature. The temperature maintained in the nozzle before the extrusion of the material is termed extrusion temperature (Figure 2).[53] It influences the viscosity of the material used for printing, thereby significantly impacting the final scaffold.[18] The temperature of the extrusion head is generally maintained at a temperature slightly higher than the melting temperature of the filament material. The melt flow behavior of the filament is substrate-specific. Polymer blends such as ABS with PMMA showed improved melt flow rates, thus improving the printing efficiency.[23] It depends on the melting temperature, thermal conductivity, rheology, specific heat, and parameters such as the velocity and nozzle size, diameter, and angle. For instance, PCL melts completely at 42 °C, and accordingly, the channel length of the extrusion head can be modified to reduce the stay time of PCL in the channel as in the current model that proves to be cost-intensive.[54] Ansari and Kamil also observed a similar effect of extrusion temperature on the flow properties of the PLA melt. It affected the final geometric correctness of the printed components. They concluded that dimensional deviation was low at higher extrusion temperatures and that the tensile property was not dependent on the extrusion temperature.[55]

3.1.3. Printing Speed. The printing speed generally refers to the amount of material deposited into an object per unit of time. 3D printers with higher speed will deposit more material over time than others. It was observed that variation in printing speeds significantly impacts the measurement accuracies.[48] Ansari and Kamil concluded that maximum tensile strength

https://doi.org/10.1021/acsomega.2c05984
ACS Omega 2023, 8, 5139−5156

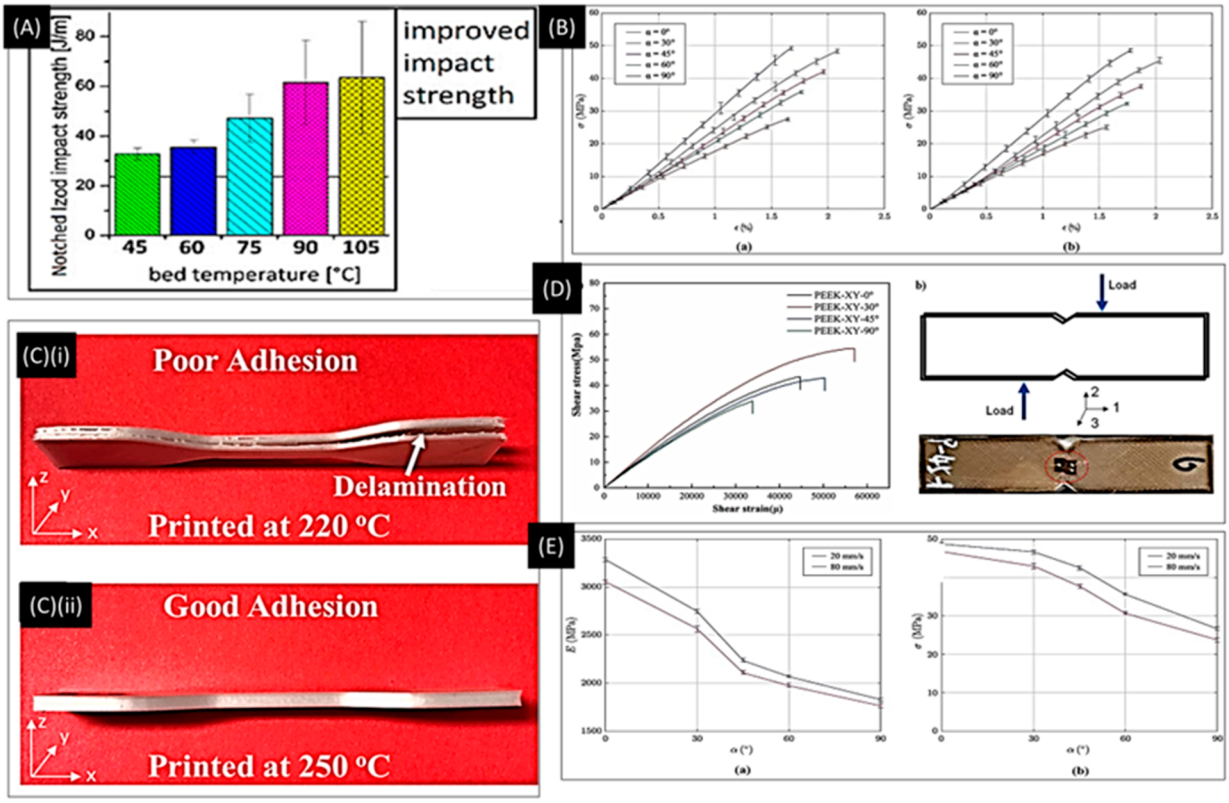

Figure 3. FDM process optimization. (A) FDM process optimization by varying temperature and raster angle. The relationship between the impact strength and bed temperature shows that with increasing temperature impact strength can be improved. Reproduced with permission from ref 70. Copyright 2018 American Chemical Society. (B) Stress−strain curves for models printed at different raster angles for speed: (a) 20 mm/s and (b) 80 mm/s. Reproduced with permission from ref 72, Open Access, CC BY 4.0. (C) (i, ii) Effect of temperature on layer adhesion. In (ii), good layer adhesion at 250° is observed. Reproduced with permission from ref 22. Copyright 2019 American Chemical Society. (D) Shear behavior with respect to various raster angles. Optimal shear characteristics are observed at 30°. Reproduced with permission from ref 73, Open Access. (E) Effect of raster direction on (a) elastic modulus and (b) tensile strength. Reproduced with permission from ref 72, Scientific Reports, Nature, CC BY 4.0

and minimum build time were achieved at higher print speeds.[55] Similarly, Narayana and Venkatesh reported better adhesion between layers at higher printing speeds due to the filling of microvoids,[56] as increasing the printing speed meant less time for the deposited layer to solidify before the deposition of the next layer, thus increasing the interlocking between the layers. However, very high print speeds were observed to affect the dimensional accuracy, resulting in voids, because higher speeds meant less time to deposit the extrudate.[56] Hence, there are possibilities of an increase in tensile strength due to increased material infill density. Although the printing speed did not directly affect the infill densities, the printing time increased with infill density.[57] However, the investigation by Miazio suggested that the strength of the samples decreased with increasing speed.[58] This might be because, at a higher print speed, vibrations of the nozzle may induce instability that can be observed as visual waves on the printed item.[59] This might be responsible for the poor interfacial bonding between the printed layers and filaments.

3.1.4. Raster Angle. The raster angle provides information about the orientation of each layer while printing the required product.[60] Various experiments have been carried out to study the influence of raster angles on the properties (Figure 2A). For instance, Wu et al. observed the effects of raster angle and layer thickness on the mechanical properties of 3D-printed PEEK samples. The authors observed the highest mechanical strengths at raster angles of 0/90°.[61] Further, Samykano et al. also concluded that maximum tensile properties for ABS 3D-printed specimens were achieved with a raster angle of 55°. These authors also concluded that a raster angle of 55° gave the highest tensile force resistance in the specimens[49] (Figure 2B). When the tensile properties of 3D-printed PLA samples with different in-plane raster angles were investigated by Ayatollahi et al., the authors observed the highest fracture resistance at an angle of 45/−45°.[62]

3.1.5. Layer Thickness. Layer thickness refers to the amount of material deposited by the nozzle onto the vertical axis of the FDM 3D printer. The diameter of the nozzle tip usually controls this parameter. Wu et al. reported that an increase in layer thickness reduced the product's strength.[61] de Toro et al. suggested a minimum layer thickness for better flexibility.[63] Nugroho et al. investigated the influence of layer thickness on the flexural strengths of PLA samples. The authors observed a decrease in the tensile strength followed by an increase with a gradual increase in layer thickness.[64] Hence, increased layer thickness in upright orientations was preferred because it ensured high tensile and flexural strength. In addition, Tsouknidas et al. found that an increase in layer thickness increases the risk of premature failures.[65] A relationship between the individual layer thickness and the surface roughness, which can be beneficial for the application in tissue engineering, was also drawn by Shilov et al.[24]

https://doi.org/10.1021/acsomega.2c05984
ACS Omega 2023, 8, 5139−5156

3.1.6. Infill Pattern and Density. The infill pattern describes the internal structure and shape of the printed component. Infill patterns also influence mechanical properties as different infill patterns provide different results for the tensile and compressive properties, thereby determining the final properties of the printed product. Infill density refers to the volume of material printed in the component. Rismalia et al. reported an increase in tensile properties and infill densities. Furthermore, the concentric pattern was observed to have the highest tensile properties.[66] This might be because of the isotropic distribution of materials in the printed component. Mishra et al. concluded that the impact energy absorption reached a maximum at 85% infill density in a PLA 3D-printed part (Figure 2C).[67]

3.1.7. Air Gaps. An air gap represents the interval between two adjacent rasters on the same layer. The air gap could be positive, negative, or even of zero value. In zero air gaps, the deposited materials touch and are in direct contact. In negative air gaps, the deposited materials partially overlap each other to form a denser structure. In positive air gaps, the deposited materials are apart and not in contact, resulting in a loosely packed structure (Figure 2D and E). Hohimer et al. concluded that air gaps played a significant role in the ultimate tensile strength of thermoplastic polyurethane.[68] Negative air gaps were observed to increase the materials' tensile strength significantly.

4. PARAMETERS AFFECTING THE PROPERTIES OF 3D-PRINTED COMPONENTS

4.1. Mechanical Properties. The printing-bed temperature and the extruder temperature played an important role in improving the interlayer adhesion and thereby the tensile strength. Benwood et al., in a study conducted on PLA printed models, found an increase in bed temperature to 105 °C from the reference 60 °C, which showed better impact strength due to better bonding between the extruded layers (Figure 3A).[70] Another study reported that the interlayer adhesion improved with nozzle temperature ranging from 180 to 230 °C and deposition plate temperatures of 70−110 °C. It was also seen that the molecular diffusion in the interlayer space at high temperatures improved the mechanical properties.[71] The elastic modulus of the component increased by >200% (Figure 3C).[71] Khosravani et al. reported that the printing speed and angle of raster orientation play a significant role in determining the mechanical properties of the PLA samples (Figure 3B). The raster orientation (α = 0°), where the individual PLA filaments coming out of the nozzle are in the direction of the applied load, showed maximum strength compared to the other orientations. This was primarily because the load was shared by all the available filaments of the sample. However, the load-bearing capacity was minimized by the raster orientation (α = 90°), where instead of filaments bearing the load, the degree of fusion between the filaments bore the load. The degree of fusion primarily depends on the printing speed where the melt-polymer coalesces with the neighboring filament before drying after oozing out from the nozzle. As a result, these samples had a lower degree of fusion with adjacent filaments that succumbed to fracture at a lower load.[72] Gao et al. conducted a detailed study on the role of raster orientation on different mechanical properties of polyether ether ketone (PEEK). They observed that a raster orientation of α = 0° leads to maximum tensile strength. However, when flexural and shear stress analyses were performed, it was observed that samples with a raster orientation of α = 30° were better than others (Figure 3D). Moreover, when they performed the microstructural analysis with X-ray diffraction (XRD), they found no change in polymer chain orientation compared to the injection-molded components. However, there was indeed a reduction in the degree of crystallinity by 70%, which might be attributed to the differential cooling of the surface and core of a filament. This decrease in crystallinity might be responsible for the compromised mechanical strength.[73] Naveed also demonstrated that infill speed and raster orientation significantly determine the sample's mechanical properties (Figure 3E). These parameters determine the degree of interconnections and void spaces between two contiguous rasters.[74] In the later studies, the authors explored the existence of several microscopic defects through extensive scanning electron microscopy (SEM) imaging postmechanical investigation. They concluded that these voids/defects resulted in mechanical fracture failure during tensile testing. Moreover, the samples with raster orientations of 45° and 90° showed minor surface defects, but the author suggested that internal voids in bulk might lead to fracture propagation.[75]

Özen et al. investigated the effect of layer thickness and degree of overlap on the porosity and microstructure (degree of overlap and cross-sectional shape of the fibers) at the microscale through experimental and computational approaches. They found that these microstructural changes manifest macroscale stiffness of the printed components.[69] The prediction of mechanical properties of components through computational methods has been conducted to date for components manufactured through conventional methods. Abdullah Aloyaydi et al. investigated the role of infill density on the flexural strength of the FDM-printed PLA components. They suggested that 80% infill density provides better flexural strength and gives higher toughness to the components. The varying infill density leads to varying micropores in the final fabricated components, which might be the potential cause of fracture failure.[76] Ouhsti and Haddadi explored the printing parameters speed, raster orientation, and extruder temperature on the mechanical properties of the printed samples. They employed ANOVA to establish a relationship between printing parameters and mechanical properties.[77] Kaveh et al. used high-impact polystyrene (HIPS) as a material in an FDM printer to optimize dimensional accuracy and internal cavity through changes in the parameters like raster (extruded) width and angle, flow rate, feed rate, and extrusion temperature.[78]

The material modification through composite formation or blending can significantly affect the mechanical properties of the 3D-printed components. To overcome PEEK's low mechanical strength during the FDM, Wang et al. incorporated glass fiber (GF) and carbon fiber (CF) fillers in PEEK in printed samples by FDM using PEEK/GF and PEEK/CF composites, respectively.[79] The mechanical properties of these samples were assessed by varying printing parameters like print speed, layer thickness, bed temperature, and others. They demonstrated that the mechanical properties of the samples were relatively higher in PEEK/GF and PEEK/CF composites as compared to pure PEEK due to the better pinning effect of the fibers.[79] Patanwala et al. used varying concentrations of CNT in the PLA extrude to have a composite that can have superior mechanical performance compared to native PLA.[80] They observed that Young's modulus was increased upon adding CNT, while tensile strength and toughness were decreased. They also tried to explain these observations based

https://doi.org/10.1021/acsomega.2c05984
ACS Omega 2023, 8, 5139−5156

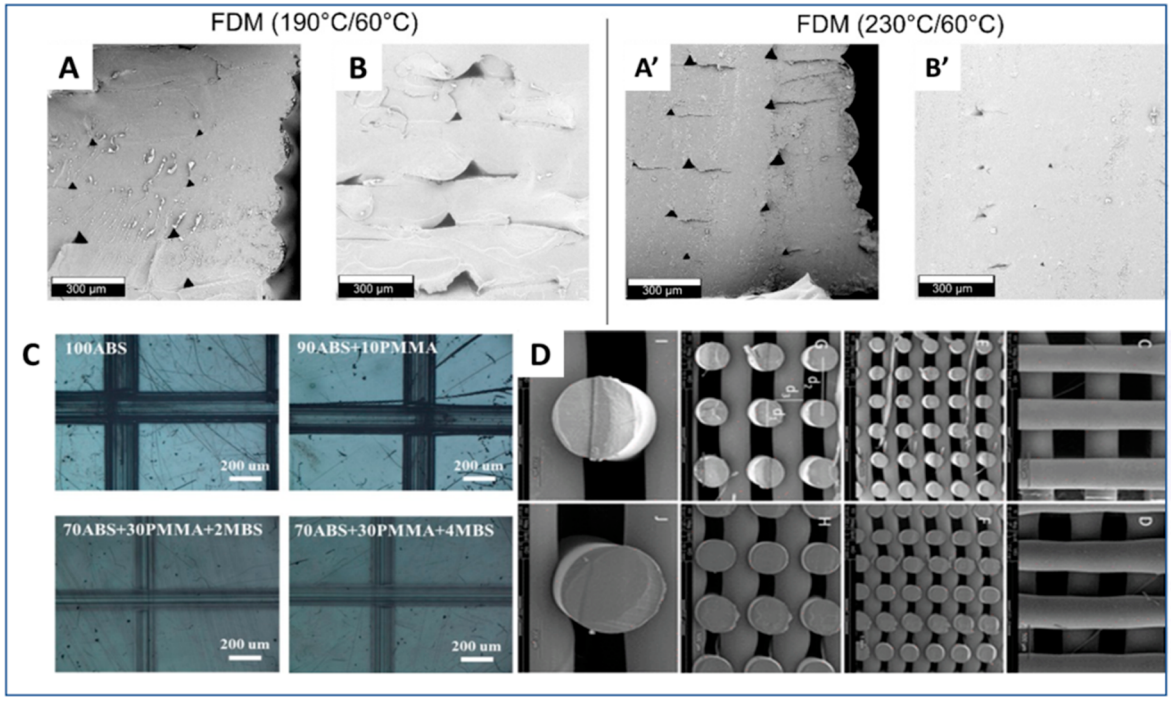

Figure 4. Effect of process parameters on the surface characteristics. (A, A', B, B') Impact of change in temperature on the surface characteristics. Reproduced with permission from ref 70. Copyright 2018 American Chemical Society. (C) Polymer blends' effect on surface properties such as scratch resistance. Reproduced with permission from ref 23. Copyright 2018 American Chemical Society. (D) Poly(ester amide) used as filament for the 3D-printed surfaces. Reproduced with permission from ref 87. Copyright 2022 American Chemical Society.

on the CNT orientation and void volume through the Halpin–Tsai model and modified and unmodified rule of mixtures (RoM) model.[81]

4.2. Surface Properties of Scaffolds. The surface features are of importance for a myriad of applications in the biomedical field. The layer-by-layer fabrication of components by FDM results in the rough morphology of the parts. This is primarily due to the partial fusion of individual molten filaments extruded from the nozzle of FDM. However, several approaches have been adopted to overcome the rough morphology and create smoothened surfaces.[82] One of the simplest ways surface smoothening was achieved was by increasing the bed temperatures and annealing postproduction (Figure 4A, A', B, and B'). Lavecchia et al. have employed ethyl acetate vapor to facilitate the fusion of surface features on the PLA components, thereby leading to a 90% reduction in surface roughness. They suggested optimization of the choice of solvent type, quantity, and treatment time to achieve better smoothening of rough surfaces.[83] Chohan et al. demonstrated that surface smoothening of FDM-printed ABS could be achieved by exposure to acetone vapors. Moreover, they observed that acetone, a harsh solvent, tends to distort the dimensions of the components upon exposure for an extended period.[84] Neff et al. utilized vapor and thermal smoothening processes to smoothen FDM-printed ABS components and later quantified the effect of achieved smoothness on the microwave noise.[85] They observed that thermal smoothening results in 80% success compared to 90% smoothening achieved by vapor treatment. Surface level modifications of the model based on vapor deposition, which is the conventional method, have numerous demerits, such as that it can change the dimension and mechanical properties. Also, smoothening due to vapor treatment may be undesirable as the leftover traces of solvent may interfere with the performance of the device or may lead to toxicity in the case of biomedical devices. Moreover, generalized surface modifications achieved by vapor deposition provide a smooth surface but do not necessarily promote cell attachment or cell proliferation.

FDM-printed scaffolds for tissue engineering applications have many specific surface-property requirements, such as surface roughness and hydrophilicity. To facilitate the cells' adhesion and proliferation, a study by Kosorn et al. treated the PCL/PHBV blended porous scaffolds with low-pressure oxygen plasma treatment (Figure 4C).[86] This resulted in increased surface wettability, surface roughness, and hydrophilicity. The authors claimed that the scaffolds could be appropriately used for cartilage tissue culture in vitro. Another study used chitosan and hydroxyapatite dispersion to modify the printed scaffold's surface to improve wettability and cell proliferation. Also, Ansari et al. suggested an amino acid-based polymer as a filament for biomedical applications.[87] They demonstrated that amino acid-based polymers elicit improved cytocompatibility and allow better amide and hydrogen bonds for better cell–scaffold interactions (Figure 4D).

5. SURFACE AND BULK FUNCTIONALIZATION FOR TISSUE ENGINEERING APPLICATION

One of the primary and crucial objectives of tissue engineering is the acceptance of the artificial tissue scaffold, the success of which relies on its resemblance with the natural 3D microenvironment. Mimicking the natural microenvironment is often necessary for proper cellular adhesion, nutrient transport, and cell–biomaterial interactions. Several functionalization methods have been reported to achieve this objective, broadly classified as bulk functionalization and surface functionalization. These functionalization techniques alter the scaffold's physical, mechanical, and chemical properties to

https://doi.org/10.1021/acsomega.2c05984
ACS Omega 2023, 8, 5139–5156

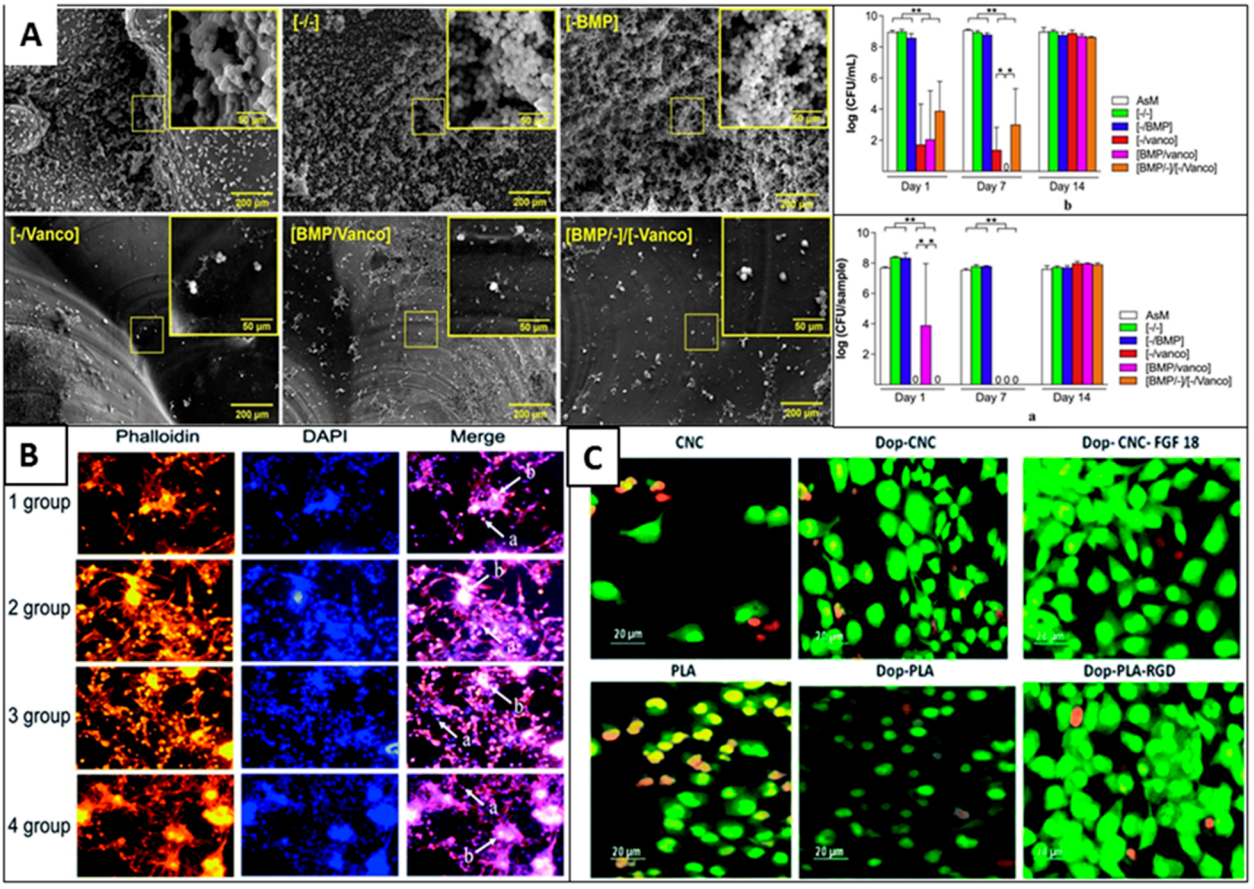

Figure 5. Biofunctionalization of scaffolds for tissue engineering applications. (A) Layer-by-layer coating of BMP and vancomycin on 3D-printed scaffolds to prevent infections and promote bone tissue engineering. Graph showing the lowering of planktonic (top) and adherent bacteria (bottom). Reproduced with permission from ref 98 (2020), Open Access, CC-BY-4.0. (B) Adhesion of islet cells on PGA scaffolds. Groups 1, 2, 3, and 4 have original PGA, plasma-treated PGA scaffold, polylysine-coated PGA scaffold, and plasma treatment combined with polylysine coating modifications, respectively. Reproduced with permission from ref 91 (2019), Open Access, CC-BY-NC. (C) Effect of dopamine coating on 3D-printed PLA scaffolds for osteoblast cell culture. Reproduced with permission from ref 99 (2020), Open Access, CC-BY-NC.

increase its biocompatibility and eventual acceptance by the body.

5.1. Surface Functionalization. The surface-functionalization methods alter the surface topography and chemical properties of the scaffold to establish better cellular interaction and improve the biocompatibility of the scaffold biomaterial. Over time, numerous physical, chemical, and biological methods for scaffold surface functionalization have been reported. Often, the objective of this functionalization is to mimic the microenvironment of the tissue to be replaced. For example, polymeric scaffolds intended to replace bone tissues are often functionalized with hydroxyapatite coating, promoting osteogenic activities for bone development and subsequent integration of the scaffold.[88] To keep the discussion concise, surface functionalization of only hard, polymeric tissue scaffolds has been emphasized.

5.1.1. Physical Methods. The physical methods primarily alter the biomimetic properties of the scaffold, such as topography, wettability, and porosity, without altering the composition of the bulk. To achieve this, various physical methods have been reported that modify the surface properties by etching at surface levels or depositing an additional active layer at the surface. Because these methods only affect the surface's physical state and do not alter the bulk scaffold's chemical composition, they are highly translatable across various types of scaffolds.[89] The topographical modifications of several hard polymeric scaffolds such as PLA, PLGA, PCL, and polystyrene have been reported.[90] These modifications are largely restricted to a few microns or nanometers from the scaffold surface. For instance, treatment of PLA scaffold with oxygen plasma has been reported to introduce surface roughness at a nanometric scale.[90] In addition, plasma treatment also generates surface hydroxyl and carboxylic acid functional groups, which increases the hydrophilicity of PLA, indicated by a reduction in the water contact angle post-treatment. The increase in surface roughness and hydrophilicity of PLA promotes cellular adhesion and proliferation (Figure 5B).[90,91] Similar plasma treatment has been reported for several different polymeric scaffolds, including poly(glycolic acid) (PGA) and PLLA, PLGA, PCL, PEO, PVDF, and PU.[92] Interestingly, various gas sources like oxygen, argon, helium, or ammonia can be used for plasma treatment, wherein each plasma type differently affects the scaffold surface properties by introducing different surface functional groups.[93,94] Similarly, physical treatment methods for 3D scaffolds include corona discharge,[95] UV irradiation,[96] and flame treatment.[97] In the corona-discharge and flame-treatment method, the polymeric scaffold surface is exposed to highly charged and ionized air molecules, which oxidize a few top layers of the polymer and generate hydrophilic functional groups.

https://doi.org/10.1021/acsomega.2c05984
ACS Omega 2023, 8, 5139−5156

Another useful method of surface modification of 3D scaffolds is the deposition/coating of an additional functional layer, which could be biologically active or useful for grafting additional layers.[100] Several physical deposition methods have been reported for surface modification, including simple physical adsorption, layer-by-layer (LBL) assembly, Langmuir−Blodgett deposition, pulse laser deposition, and ion beam deposition. Physical adsorption is the simplest of all the other approaches and usually involves the adsorption of a bioactive layer over the 3D scaffold surface by a simple immersion technique. Proteins such as collagen, laminin, integrin, fibronectin, and gelatin are routinely utilized as bioactive layers for surface functionalization, improving cellular adhesion, and scaffold acceptability. In physical adsorption, the chemical properties of both the scaffold and bioactive layer are not altered. The surface adsorption is driven by noncovalent interactions such as van der Waals interaction, electrostatic, hydrophobic, and hydrogen bonding. Despite its simplicity, one major limitation of physical adsorption is that protein molecules are randomly oriented on the scaffold surface, leading to functionality loss.[101]

Several bioactive molecules are charged species, such as hyaluronic acid, collagen, gelatin, and many more, at the physiological approach, which could be electrostatically assembled (Figure 5A).[98,102] Taking advantage of this fact, the thin-film coating of bioactive molecules over the 3D scaffold surface has been achieved by depositing oppositely charged molecules in a layer-by-layer (LBL) fashion.[103] Compared to simple physical adsorption, the LBL approach provides greater film thickness, orientation, and surface charge freedom.[104] Apart from electrostatic charge, other noncovalent interactions, such as hydrogen bonding, coordination chemistry interaction, hydrophobic interaction, and charge-transfer interaction, are also suitable for creating layer-by-layer deposition.[105] Langmuir−Blodgett (LB) deposition is another unique technique to functionalize 3D scaffolds, particularly with amphiphilic block copolymers.[106107] In contrast to other deposition techniques, LB deposition occurs in a liquid−air interface and vertical direction (Figure 6).[108] The deposition takes place due to the physical adsorption of the bioactive layer dispersed in the liquid phase onto the solid substrate. Interestingly, the deposition technique not only provides precise control over the layer thickness but also allows control over the orientation, packing density, and polarity (hydrophobic/hydrophilic) of the deposited film.[109,110]

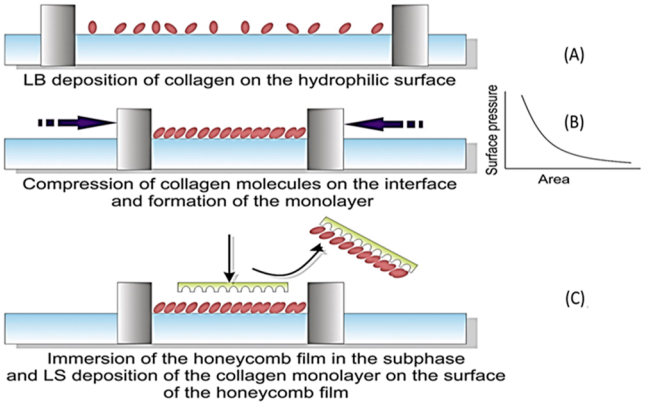

Figure 6. LB deposition of collagen layer on poly(L-*co*-D,L-lactic acid) PLDLA substrate. Adapted with permission from ref 111. Copyright 2017 Elsevier.

5.1.2. Chemical Methods. Unlike physical methods of functionalization, chemical methods alter the chemical properties of the scaffold surface by covalent modifications. Chemical functionalization methods include wet chemical etching,[112] polarity reversal by solvent or partial solvent exposure,[113] and covalent grafting.[114] In wet chemical etching, the covalent bonds of the polymer scaffold are subjected to acid or alkali hydrolysis, resulting in surface oxidation and introducing different chemical functional groups like carboxylic acid, hydroxyl, and aldehyde groups. For instance, surface ester bonds of poly-L-lactic acid (PLLA) scaffolds can be easily broken through alkali/acid hydrolysis.[115] Subsequent treatment with citric acid improved surface hydrophilicity and introduced porosity.[116] In another comparison between oxygen plasma-treated and wet chemical-treated 3D scaffolds of PLA, it was found that chemical etching generates a higher number of surface functional groups (carboxylic acid) and higher porosity than the plasma-treated scaffolds.[90] The etching parameters can be easily varied by changing the temperature, type, and concentration of the alkali/acid, etc. However, despite its simplicity, one major disadvantage of wet chemical etching is the uncontrolled oxidation and introduction of various oxygen functional groups on the scaffold surface. As a result, the process is generally nonreproducible and therefore limited to research laboratories. Furthermore, the process also generated much hazardous chemical waste, which is not amiable for industry-level scale-up.

Generally, polymers like PLLA and poly-D,L-lactic-*co*-glycolic acid (PLGA) routinely used for 3D scaffold preparation are insoluble in most common solvents. However, it has been found that exposure of 3D scaffolds of PLLA or PLGA to certain solvents such as toluene, ethyl acetate, and acetone has a dramatic and long-lasting effect on its surface hydrophobicity. These solvents swell the surface of the scaffold-like hydrogel without dissolving the polymer itself and thus present an excellent opportunity for surface entrapment.[113] Using this approach, the surface of PLLA scaffolds was modified with heparin molecules and evaluated by platelet adhesion.[117]

The covalent grafting of various bioactive molecules and polymers over the 3D scaffold surface has been one of the most extensively explored functionalization routes. Because of strong covalent bonds for adsorption, the deposited layer firmly adheres to the surface. Covalent grafting is also biocompatible in terms of promoting cellular growth under body fluid flow conditions. The covalent binding of the additional polymer or bioactive layer can be accomplished by chemical ligation or a photochemical reaction induced by UV radiation. For instance, Chatterjee et al. reported the grafting of low molecular weight PEI onto the surface of a PLA 3D scaffold by well-known EDC/NHS coupling chemistry.[118] Before the coupling, the scaffold was treated with alkali hydrolysis to introduce the carboxylic acid functional group. After PEI grafting, the scaffold was chemically grafted with citric acid and finally functionalized with calcium phosphate. As a result of this modification, the scaffold exhibited enhanced surface roughness and hydrophilicity and promoted enhanced stem cell adhesion and proliferation compared with the control (untreated) scaffold.[119] The high-energy UV radiation can also be utilized for photochemical ligation of the active layer over the scaffold surface. Two different approaches have been reported for UV-induced grafting.[114] The whole polymer is

https://doi.org/10.1021/acsomega.2c05984
ACS Omega 2023, 8, 5139−5156

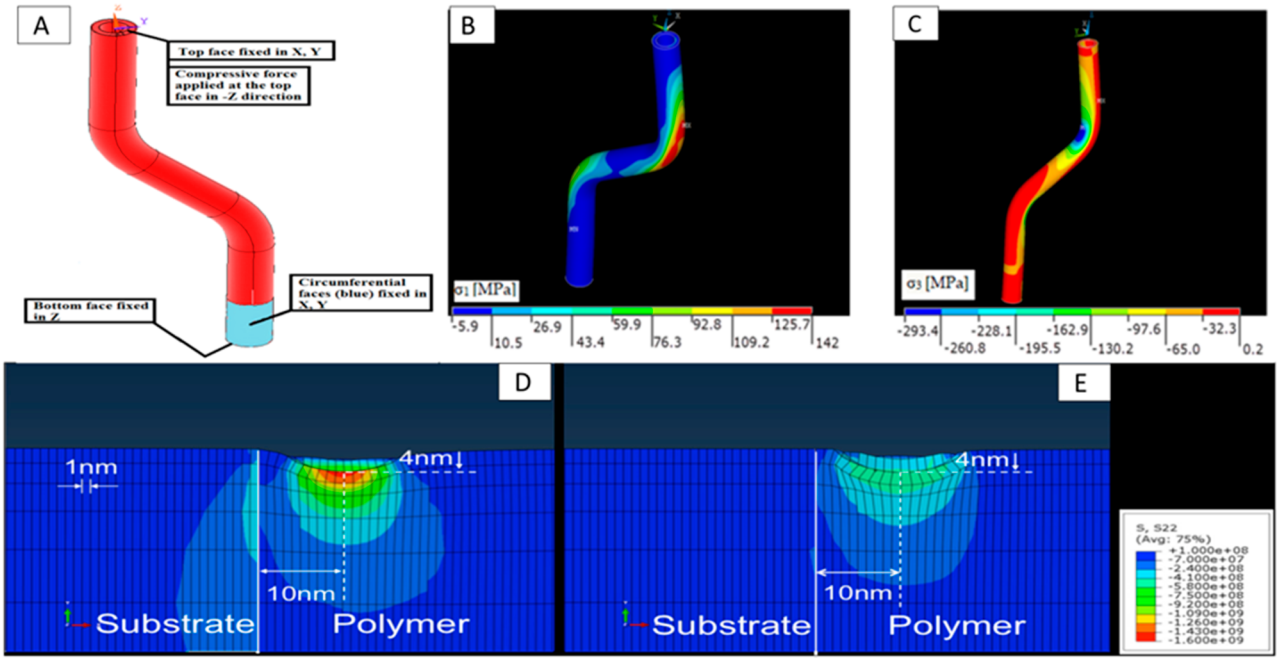

Figure 7. (A−C) FEM analysis of the application of compressive mechanical stress on a 3D-printed hollow fiber. Reproduced with permission from ref 125. Copyright 2021 MDPI. (D, E) Simulating the stress field effect upon indentation at substrate−polymer interface of an FDM 3D-printed surface. In (D), the polymer is purely elastic, and in (E), it is a blend of elastic−plastic model polymers. Reproduced with permission from ref 128. Copyright 2018 American Chemical Society.

ligated over the scaffold surface in one approach. For instance, vapor-phase photografting of PLA scaffold with polyacrylic acid (PAA), poly(methyl acrylate) (PMA), and poly-(vinylpyrrolidone) (PVP) was reported by Albertsson and co-workers.[120] The vapor-phase reaction ensured uniform distribution of the grafted polymers and prevented solvent effects on the scaffold. However, because of steric hindrance and diffusional limitations of whole polymers, the high packing density of graft polymer at the scaffold surface is challenging to achieve. In the second approach, the graft polymer is grown at the scaffold surface from its photoactive monomers by photopolymerization. For example, after surface activation of PLA scaffold by argon-plasma treatment, a hydrophilic polymer brush of PAA has been grown at the scaffold surface by photopolymerization of acrylic acid monomer. The UV radiation using benzophenone as a photoinitiator is used for photopolymerization.[121] The second method provides a high degree of control over the scaffold surface's chemical properties, with the only disadvantage being immobilizing the photoinitiator at the scaffold surface.

The scaffold surface is often functionalized with bioactive molecules such as proteins, peptides, growth factors, minerals, etc. to mimic the target tissue's microenvironment and increase the scaffold's acceptability.[122] The functionalization of bioactive molecules also imparts enhanced biocompatibility to the scaffold. For example, surface functionalization of PLA scaffold with fibroblast growth factor (FGF-18) and arginyl-glycyl-aspartic acid (RGD) peptide increases cell adhesion and proliferation. The functionalized scaffolds also exhibit improved blood compatibility and antimicrobial activity (Figure 5C).[99] Similarly, mineralization of scaffolds with calcium phosphate or functionalization with hydroxyapatite (HA) has been reported to promote osteogenic activity and easy integration into bone tissue.[123124]

6. MODELING AND SIMULATION AID FOR PERFORMANCE EVALUATION

3D printing of a structure using FDM technology depends on many variables leading to the physical and mechanical characteristics of the printed material. Experimental parameter optimization is a lengthy, time-consuming, tedious, and cumbersome process. With the advent of simulation technology, such as finite element modeling, this process can be accomplished with minimal time and resources, making it a helpful tool for researchers working with 3D-printed materials.

The mechanical characteristics of the 3D-printed materials can be determined with precise accuracy using the finite element method analysis, as was substantiated by a study conducted to test the tensile strength of an FDM-printed hollow off-axis profile with carbon fiber-reinforced polymer filament[125] (Figure 7A−C). Moreover, optimizing the consequential operating parameters can lead to developing materials with better compressive, tensile, and fracture strength. Temperature is an important determinant operating parameter that can lead to mechanical defects such as poor bonding, wrinkling, and warpage of the printed material.[15] Nonuniform shrinkage in the internal parts and no effect on the sides in response to the rapid heating and cooling occur during the printing process, leading to the warping of the part. Finite element modeling was performed to determine the tensile strength of the printed material, and Taguchi's model was used to identify the significant process parameters. Significant parameters, i.e., model layer's thickness and bed temperature, were chosen for the application through ANSYS. Although the present model tends to overestimate the defect, the error percentage is relatively low.[15] Another defect commonly observed in 3D-printed materials of PLA is low isotopic fracture strength because of the low adhesion strength between the adjacent layers, which leads to fracture on the application of load. The scaffold's fracture strength was

https://doi.org/10.1021/acsomega.2c05984
ACS Omega 2023, 8, 5139−5156

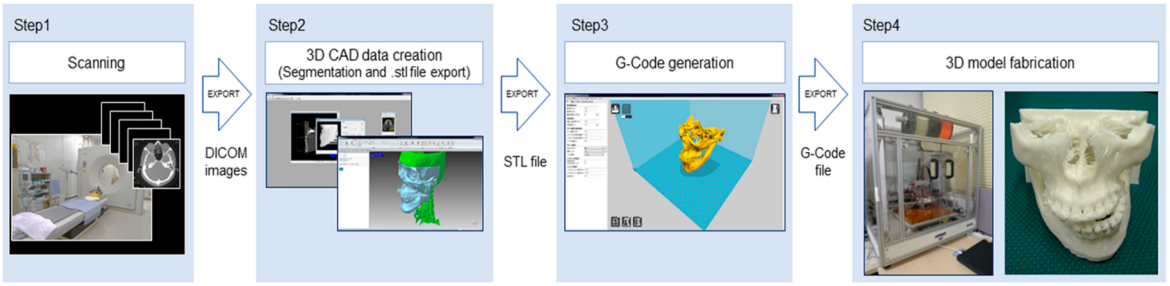

Figure 8. Process workflow for fabricating a patient-specific 3D scaffold. Reprinted with permission from ref 138 (2020), Open Access.

bettered by 1400% by optimizing the process parameters.[126] Mechanical strength is directly related to the interlayer bond strength, which is, in turn, a measure of free molecular diffusion at the interface.[127] The nozzle temperature and the print-bed temperature optimization led to better adhesion between the two adjacent printed layers. This was successfully proven in an FEM simulation-based study to better the mechanical properties of PLA models printed by FDM.[71] The effect of polymer blends on mechanical properties has also been studied using stress field simulation to improve the strength of the printed component (Figure 7D and E).[128]

Polymer melting inside the extruder is the first step in the FDM-printing process, and the melt flow behavior is optimized using representative biomaterial PCL in terms of temperature, nozzle diameter, angle, flow velocity, channel width, and length, leading to a mechanically more stable scaffold designed for tissue engineering.[129] So, the lamellate theory has been adopted to predict the mechanical behavior of 3D-printed components as the fusion of different layers of materials forms the components. However, Nasirov et al. suggested that lamellate theory may not be sufficient to predict mechanical behavior accurately.[130] Hence, they suggested that multiscale modeling coupled with lamellate theory will likely yield a better prediction approach. Theoretical process parameter optimizations through mathematical models have been investigated experimentally. On the other hand, simulation models have been developed based on experimental results that were used to substantiate the mathematical models and theoretical predictions. This interdependence paved the path for faster and sometimes unconventional advancements in FDM-based 3D printing.

7. APPLICATIONS OF FDM IN TISSUE ENGINEERING

Fused deposition modeling (FDM) has garnered tremendous interest in various technological and biomedical industries in the past few years. The ease of rapid, on-site, and on-demand fabrication of scaffolds with intricate designs and the availability of a wide range of low-cost raw materials (thermoplastics) have helped FDM establish itself as one of the leading technologies in the rapid printing/prototyping field. Therefore, it is not surprising to find several applications of FDM prototyping in several biomedical fields, such as scaffolds for bone tissue engineering, craniofacial tissue engineering, and fabrication of implants and stents.[131] Despite its commercial success in various other technological industries, one of the limiting challenges of FDM in the biomedical field is the availability of very few biocompatible thermoplastics. Only a handful of thermoplastics, such as PCL, PLLA, PLA, PLGA, and PEEK, are suitable for FDM 3D printing for biomedical purposes. Among these, PCL has been extensively explored for bone tissue engineering applications due to its biocompatibility, slow biodegradation, and low toxicity of byproducts generated during metabolism. The FDA has also approved PCL for clinical applications. In general, the scaffolds prepared by PCL are hydrophobic, which is suitable for cellular adhesion and proliferation.[132] Thus, PCL scaffolds are often functionalized postfabrication through various surface-functionalization routes.[132] Another useful approach to functionalizing PCL scaffolds is to use composite filaments during 3D printing. For example, incorporating bioceramics such as hydroxyapatite and beta-tricalcium phosphates during 3D printing has improved the mechanical properties of scaffolds and promoted osteogenic properties.[133−135]

Another biomedical application of FDM included craniofacial tissue engineering, which includes the periodontal complex, dental pulp, and alveolar bone and cartilage.[136] In an interesting study, Kim et al. fabricated a 3D scaffold resembling anatomically human molar teeth from PCL and hydroxyapatite with 200 μm interconnecting microchannels.[136] The microchannels were loaded with stromal-derived factor-1 (SDF-1) and bone morphogenic protein-7 (BMP-7). After in vivo study in rats for 9 weeks, the scaffold could recruit more endogenous cells and promote higher angiogenesis than the control scaffold (Figure 8). In a similar study, Li et al. fabricated a 3D scaffold of PCL and functionalized it with freeze-dried platelet-rich plasma (PRP). Compared with the nonfunctionalized one, the PRP scaffold promoted enhanced cellular interaction with dental pulp stem cells (DPSC), upregulated the mRNA expression of osteogenic genes, and enhanced bone formation.[137]

The versatility of the FDM approach also makes it suitable for the fabrication of tailored/customizable implants, such as those required in reconstructive surgeries. Aided by computational programs, a patient-specific reconstructive implant with intricate geometry can easily be fabricated for aesthetic purposes or to restore mechanical or respiratory functions after major accidents.[139] In a similar study, He et al. fabricated an extravascular PEEK stent to treat nutcracker syndrome.[140] The patients underwent laparoscopic surgeries, and the FDM-fabricated 3D stent was fitted in vivo to resolve the symptoms. The stent performed exceptionally well, and the symptoms of all of the patients were resolved. In 3−6 months of follow-up studies, the stents were visualized through CT and Doppler ultrasound studies and showed no migration or thrombosis. Compared with polytetrafluoroethylene (PTFE) or endovascular stents, the fabricated PEEK stents exhibited improved design and rigidity without any side effects.

https://doi.org/10.1021/acsomega.2c05984
ACS Omega 2023, 8, 5139−5156

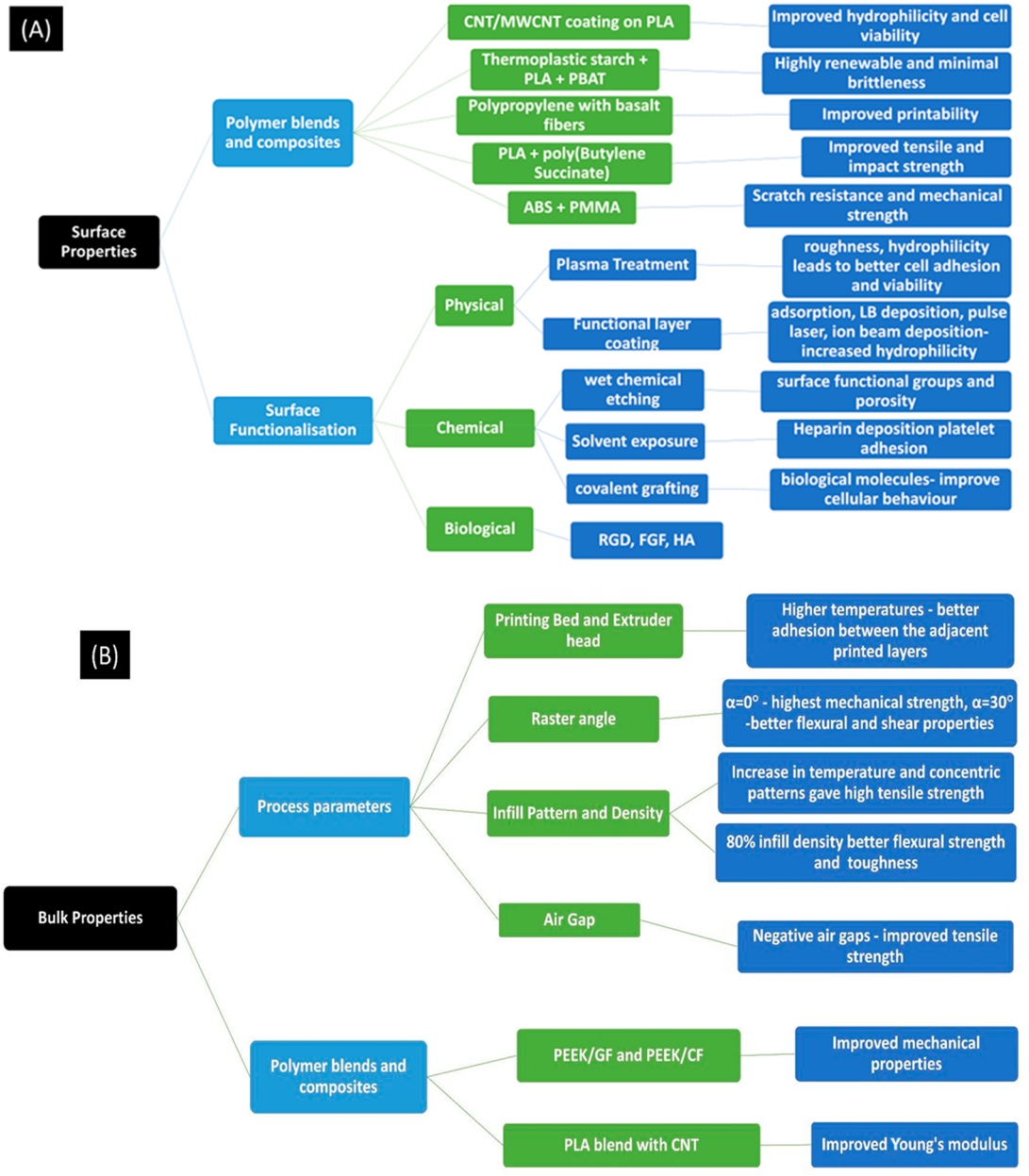

Figure 9. (A, B) Summary of surface and bulk parameters improved for tissue engineering applications through changes in process parameters and 3D-printer properties.

8. CONCLUSION AND FUTURE WORK

FDM 3D printing melts the polymer in the extruder head and prints the desired structure, digitally designed in a layer-by-layer fashion on a flat support structure. Although it is a straightforward and efficient technique for generating accurate structures suitable for the automobile to the biomedical industries, it inherently produces mechanically weak structures. This is because of the uneven cooling and shrinkage of different parts of the same structure, thereby making it vulnerable to stress. Through this review, we have tried to understand the process of 3D printing and identify the different significant process parameters to bring about the necessary surface and bulk properties to generate accurate designs and make them mechanically strong and stable. Over the past decade, FDM 3D printers have gone through multiple advancements, further simplifying printer designs. Taguchi's modeling was a critical numerical method that aided in the identification of significant printing process parameters and optimizing their value. The print-bed and extruder-head temperatures influence the adjacent interlayer adhesion and their mechanical strength in terms of compression, fracture, and tensile strength. Layer thickness, infill pattern, raster angle, and printing speed are crucial in determining mechanical characteristics.

Filament for 3D-printed models is generally made of acetonitrile butadiene styrene (ABS), polyether ether ketone (PEEK), poly(lactic acid) (PLA), and sometimes polycaprolactone (PCL), etc. However, they showed demerits such as low mechanical strength and limited cell adhesion and growth. Polymer blends, including nanocomposites, and surface functionalization using bioceramics and proteins provide a biomimicking microenvironment that drastically improves behavior in response to cells. We have, in this study,

https://doi.org/10.1021/acsomega.2c05984
ACS Omega 2023, 8, 5139−5156

extensively discussed the different methods of functionalization and bioactive molecules deposited on the surface that increase the cell's affinity toward the FDM 3D-printed scaffold (summarized in Figure 9A and B). Simulation technology is another newer technology that, in recent years, has allowed for faster, less cost-intensive, and more efficient methods to determine the optimal level of the significant process parameters and optimize the printing process of a system. Polymers such as PCL, PLLA, PLA, PLGA, and PEEK have found their applicability not only in tissue engineering for the periodontal complex, dental pulp, and alveolar bone and cartilage but also in the development of patient-specific implants owing to the special ability of FDM 3D printing to produce highly customizable and design-oriented models.

FDM 3D printers have a long way ahead in biomedical engineering and can be used for large-scale prototyping with the advent of crucial and directed interdisciplinary advancements. Further optimization of the 3D printer design and process parameters will be able to cater to varied and improved filaments and their differential specific melting temperatures. Advancements in artificial intelligence will prove to be a boon in the revolutionizing of 3D printing by optimizing the process parameters according to the need, thus ensuring better surface and bulk properties in the printed model. Moreover, FDM 3D printers currently allow printing on flat support structures; we predict a more customized printing technology will be developed that will also be powered by artificial intelligence.

AUTHOR INFORMATION

Corresponding Authors

Prasoon Kumar − *Biodesign and Medical Device Laboratory, Department of Biotechnology and Medical Engineering, National Institute of Technology, Rourkela 769008, India*; orcid.org/0000-0003-0854-3889; Email: kumarprasoon@nitrkl.ac.in, prasoonkumar1985@gmail.com

Girish Chandra Mohanta − *Materials Science and Sensor Applications Division, CSIR−Central Scientific Instruments Organizations (CSIR-CSIO), Chandigarh 160030, India*; Email: gmohanta@csio.res.in

Authors

Ruchira Chakraborty − *Biodesign and Medical Device Laboratory, Department of Biotechnology and Medical Engineering, National Institute of Technology, Rourkela 769008, India*

Abhijeet Govind Anoop − *Biodesign and Medical Device Laboratory, Department of Biotechnology and Medical Engineering, National Institute of Technology, Rourkela 769008, India*

Abhay Thakur − *Biodesign and Medical Device Laboratory, Department of Biotechnology and Medical Engineering, National Institute of Technology, Rourkela 769008, India*

Complete contact information is available at: https://pubs.acs.org/10.1021/acsomega.2c05984

Notes

The authors declare no competing financial interest.

ACKNOWLEDGMENTS

R.C. thanks NIT Rourkela for funding her Ph.D. scholarship. P.K. thanks the Science and Engineering Research Board (SERB), Department of Science and Technology, Government of India, for financial support through SRG/2021/000859.

ABBREVIATIONS

FDM	Fused deposition modeling
PLA	Poly(lactic acid)
CNT	Carbon nanotubes
HA/HAp	Hydroxyapatite
PCL	Polycaprolactone
PEEK	Polyether ether ketone
ABS	Acetonitrile butadiene styrene
PBAT	Polybutylene adipate terephthalate
TPS	Thermoplastic starch
PMMA	Poly(methyl methacrylate)
CNC	Computer numerical control
PLGA	Poly-D,L-lactic-*co*-glycolic acid
PLLA	Poly-L-lactic acid
PEO	Poly(ethylene oxide)
PVDF	Poly(vinylidene fluoride)
PU	Polyurethane
PHBV	Polyhydroxybutyrate-*co*-hydroxy valerate
PLD	Pulsed laser deposition
IBD	Ion beam deposition
IBAD	Ion beam-assisted deposition
PEI	Polyethylenimine
EDC/NHS	Ethyl(dimethylaminopropyl)carbodiimide/*N*-hydroxysuccinimide
PAA	Polyacrylic acid
PMA	Poly(methyl acrylate)
PVP	Poly(vinylpyrrolidone)
RGD	Arginyl-glycyl-aspartic acid
FGF	Fibroblast growth factor
FEM	Finite element modeling
FDA	Food and Drug Administration
BMP	Bone morphogenic protein-7
SDF-1	Stromal-derived factor-1

REFERENCES

(1) Redaelli, D. F.; Abbate, V.; Storm, F. A.; Ronca, A.; Sorrentino, A.; de Capitani, C.; Biffi, E.; Ambrosio, L.; Colombo, G.; Fraschini, P. 3D Printing Orthopedic Scoliosis Braces: A Test Comparing FDM with Thermoforming. *Int. J. Adv. Manuf. Technol.* **2020**, *111* (5−6), 1707−1720.

(2) Yu, N.; Sun, X.; Wang, Z.; Zhang, D.; Li, J. Effects of Auxiliary Heat on the Interlayer Bonds and Mechanical Performance of Polylactide Manufactured through Fused Deposition Modeling. *Polym. Test* **2021**, *104*, 107390.

(3) Singh, G.; Singh, S.; Prakash, C.; Kumar, R.; Kumar, R.; Ramakrishna, S. Characterization of Three-Dimensional Printed Thermal-Stimulus Polylactic Acid-Hydroxyapatite-Based Shape Memory Scaffolds. *Polym. Compos* **2020**, *41* (9), 3871−3891.

(4) Jensen, J.; Rölfing, J. H. D.; Svend Le, D. Q.; Kristiansen, A. A.; Nygaard, J. V.; Hokland, L. B.; Bendtsen, M.; Kassem, M.; Lysdahl, H.; Bünger, C. E. Surface-Modified Functionalized Polycaprolactone Scaffolds for Bone Repair: In Vitro and in Vivo Experiments. *J. Biomed Mater. Res. A* **2014**, *102* (9), 2993−3003.

(5) Haryńska, A.; Carayon, I.; Kosmela, P.; Szeliski, K.; Łapiński, M.; Pokrywczyńska, M.; Kucińska-Lipka, J.; Janik, H. A Comprehensive Evaluation of Flexible FDM/FFF 3D Printing Filament as a Potential Material in Medical Application. *Eur. Polym. J.* **2020**, *138*, 109958.

(6) Saini, P.; Arora, M.; Kumar, M. N. V. R. Poly(Lactic Acid) Blends in Biomedical Applications. *Adv. Drug Deliv Rev.* **2016**, *107*, 47−59.

(7) Han, X.; Yang, D.; Yang, C.; Spintzyk, S.; Scheideler, L.; Li, P.; Li, D.; Geis-Gerstorfer, J.; Rupp, F. Carbon Fiber Reinforced PEEK

Composites Based on 3D-Printing Technology for Orthopedic and Dental Applications. *J. Clin Med.* **2019**, *8* (2), 240.
(8) Pentek, A.; Nyitrai, M.; Schiffer, A.; Abraham, H.; Bene, M.; Molnar, E.; Told, R.; Maroti, P. The Effect of Printing Parameters on Electrical Conductivity and Mechanical Properties of PLA and ABS Based Carbon Composites in Additive Manufacturing of Upper Limb Prosthetics. *Crystals 2020, Vol. 10, Page 398* **2020**, *10* (5), 398.
(9) Silva, E.; de Vasconcellos, L. M. R.; Rodrigues, B. V. M.; dos Santos, D. M.; Campana-Filho, S. P.; Marciano, F. R.; Webster, T. J.; Lobo, A. O. PDLLA Honeycomb-like Scaffolds with a High Loading of Superhydrophilic Graphene/Multi-Walled Carbon Nanotubes Promote Osteoblast in Vitro Functions and Guided in Vivo Bone Regeneration. *Mater. Sci. Eng.: C* **2017**, *73*, 31−39.
(10) Kotsilkov, S.; Ivanov, E.; Vitanov, N. K. Release of Graphene and Carbon Nanotubes from Biodegradable Poly(Lactic Acid) Films during Degradation and Combustion: Risk Associated with the End-of-Life of Nanocomposite Food Packaging Materials. *Materials 2018, Vol. 11, Page 2346* **2018**, *11* (12), 2346.
(11) Tian, L.; Zhang, Z.; Tian, B.; Zhang, X.; Wang, N. Study on Antibacterial Properties and Cytocompatibility of EPL Coated 3D Printed PCL/HA Composite Scaffolds. *RSC Adv.* **2020**, *10* (8), 4805−4816.
(12) N'deh, K. P. U.; Kim, G. J.; Chung, K. H.; Shin, J. S.; Lee, K. S.; Choi, J. W.; Lee, K. J.; An, J. H. Surface-Modified Industrial Acrylonitrile Butadiene Styrene 3D Scaffold Fabrication by Gold Nanoparticle for Drug Screening. *Nanomaterials (Basel)* **2020**, *10* (3), 529.
(13) Fazeli, N.; Arefian, E.; Irani, S.; Ardeshirylajimi, A.; Seyedjafari, E. 3D-Printed PCL Scaffolds Coated with Nanobioceramics Enhance Osteogenic Differentiation of Stem Cells. *ACS Omega* **2021**, *6* (51), 35284−35296.
(14) Han, X.; Yang, D.; Yang, C.; Spintzyk, S.; Scheideler, L.; Li, P.; Li, D.; Geis-Gerstorfer, J.; Rupp, F. Carbon Fiber Reinforced PEEK Composites Based on 3D-Printing Technology for Orthopedic and Dental Applications. *J. Clin Med.* **2019**, *8* (2), 240.
(15) Syrlybayev, D.; Zharylkassyn, B.; Seisekulova, A.; Perveen, A.; Talamona, D. Optimization of the Warpage of Fused Deposition Modeling Parts Using Finite Element Method. *Polymers* **2021**, *13* (21), 3849.
(16) Sacks, D.; Baxter, B.; Campbell, B. C. V.; Carpenter, J. S.; Cognard, C.; Dippel, D.; Eesa, M.; Fischer, U.; Hausegger, K.; Hirsch, J. A.; Hussain, M. S.; Jansen, O.; Jayaraman, M. v.; Khalessi, A. A.; Kluck, B. W.; Lavine, S.; Meyers, P. M.; Ramee, S.; Rüfenacht, D. A.; Schirmer, C. M.; Vorwerk, D. Multisociety Consensus Quality Improvement Revised Consensus Statement for Endovascular Therapy of Acute Ischemic Stroke. *Int. J. Stroke* **2018**, *13* (6), 612−632.
(17) Kristiawan, R. B.; Imaduddin, F.; Ariawan, D.; Ubaidillah; Arifin, Z. A Review on the Fused Deposition Modeling (FDM) 3D Printing: Filament Processing, Materials, and Printing Parameters. *Open Engineering* **2021**, *11*, 639−649.
(18) Solomon, I. J.; Sevvel, P.; Gunasekaran, J. A Review on the Various Processing Parameters in FDM. In *Materials Today: Proceedings*; Elsevier, Ltd.: 2020; Vol. *37*, pp 509−514; DOI: 10.1016/j.matpr.2020.05.484.
(19) Kim, K.; Park, J.; Suh, J.; Kim, M.; Jeong, Y.; Park, I. 3D Printing of Multiaxial Force Sensors Using Carbon Nanotube (CNT)/Thermoplastic Polyurethane (TPU) Filaments. *Sens. Actuators, A* **2017**, *263*, 493−500.
(20) Sciancalepore, C.; Togliatti, E.; Marozzi, M.; Rizzi, F. M. A.; Pugliese, D.; Cavazza, A.; Pitirollo, O.; Grimaldi, M.; Milanese, D. Flexible PBAT-Based Composite Filaments for Tunable FDM 3D Printing. *ACS Appl. Bio Mater.* **2022**, *5*, 3219.
(21) Ju, Q.; Tang, Z.; Shi, H.; Zhu, Y.; Shen, Y.; Wang, T. Thermoplastic Starch Based Blends as a Highly Renewable Filament for Fused Deposition Modeling 3D Printing. *Int. J. Biol. Macromol.* **2022**, *219*, 175−184.
(22) Qahtani, M.; Wu, F.; Misra, M.; Gregori, S.; Mielewski, D. F.; Mohanty, A. K. Experimental Design of Sustainable 3D-Printed Poly(Lactic Acid)/Biobased Poly(Butylene Succinate) Blends via Fused Deposition Modeling. *ACS Sustain Chem. Eng.* **2019**, *7* (17), 14460−14470.
(23) Chen, S.; Lu, J.; Feng, J. 3D-Printable ABS Blends with Improved Scratch Resistance and Balanced Mechanical Performance. *Ind. Eng. Chem. Res.* **2018**, *57* (11), 3923−3931.
(24) Shilov, S. Y.; Rozhkova, Y. A.; Markova, L. N.; Tashkinov, M. A.; Vindokurov, I. v.; Silberschmidt, V. v. Biocompatibility of 3D-Printed PLA, PEEK and PETG: Adhesion of Bone Marrow and Peritoneal Lavage Cells. *Polymers 2022, Vol. 14, Page 3958* **2022**, *14* (19), 3958.
(25) Nevado, P.; Lopera, A.; Bezzon, V.; Fulla, M. R.; Palacio, J.; Zaghete, M. A.; Biasotto, G.; Montoya, A.; Rivera, J.; Robledo, S. M.; Estupiñan, H.; Paucar, C.; Garcia, C. Preparation and in Vitro Evaluation of PLA/Biphasic Calcium Phosphate Filaments Used for Fused Deposition Modelling of Scaffolds. *Materials Science and Engineering: C* **2020**, *114*, 111013.
(26) Nazan, M. A.; Ramli, F. R.; Alkahari, M. R.; Abdullah, M. A.; Sudin, M. N. An Exploration of Polymer Adhesion on 3D Printer Bed. In *IOP Conference Series: Materials Science and Engineering*; Institute of Physics Publishing: 2017; Vol. *210*; DOI: 10.1088/1757-899X/210/1/012062.
(27) Sun, W.; Feinberg, A.; Webster-Wood, V. Continuous Fiber Extruder for Desktop 3D Printers toward Long Fiber Embedded Hydrogel 3D Printing. *HardwareX* **2022**, *11*, e00297.
(28) Pusch, K.; Hinton, T. J.; Feinberg, A. W. Large Volume Syringe Pump Extruder for Desktop 3D Printers. *HardwareX* **2018**, *3*, 49−61.
(29) Ali, M. H.; Mir-Nasiri, N.; Ko, W. L. Multi-Nozzle Extrusion System for 3D Printer and Its Control Mechanism. *International Journal of Advanced Manufacturing Technology 2015 86:1* **2016**, *86* (1), 999−1010.
(30) Hachimi, T.; Naboulsi, N.; Majid, F.; Rhanim, R.; Mrani, I.; Rhanim, H. Design and Manufacturing of a 3D Printer Filaments Extruder. *Procedia Structural Integrity* **2021**, *33* (C), 907−916.
(31) Arefin, A. M. E.; Khatri, N. R.; Kulkarni, N.; Egan, P. F. Polymer 3D Printing Review: Materials, Process, and Design Strategies for Medical Applications. *Polymers* **2021**, *13* (9), 1499.
(32) Šljivic, M.; Pavlovic, A.; Kraišnik, M.; Ilić, J. Comparing the Accuracy of 3D Slicer Software in Printed Enduse Parts. In *IOP Conference Series: Materials Science and Engineering*; Institute of Physics Publishing: 2019; Vol. *659*, 012082; DOI: 10.1088/1757-899X/659/1/012082.
(33) Ismail, R.; Taqriban, R. B.; Ariyanto, M.; Atmaja, A. T.; Sugiyanto; Caesarendra, W.; Glowacz, A.; Irfan, M.; Glowacz, W. Affordable and Faster Transradial Prosthetic Socket Production Using Photogrammetry and 3D Printing. *Electronics 2020, Vol. 9, Page 1456* **2020**, *9* (9), 1456.
(34) Blok, L. G.; Longana, M. L.; Yu, H.; Woods, B. K. S. An Investigation into 3D Printing of Fibre Reinforced Thermoplastic Composites. *Addit. Manuf.* **2018**, *22*, 176−186.
(35) Karakurt, I.; Lin, L. 3D Printing Technologies: Techniques, Materials, and Post-Processing. *Curr. Opin. Chem. Eng.* **2020**, *28*, 134−143.
(36) Polamaplly, P.; Cheng, Y.; Shi, X.; Manikandan, K.; Kremer, G. E.; Qin, H. 3D Printing and Characterization of Hydroxypropyl Methylcellulose and Methylcellulose for Biodegradable Support Structures. *Procedia Manuf.* **2019**, *34*, 552−559.
(37) Nisser, M.; Zhu, J.; Chen, T.; Bulovic, K.; Punpongsanon, P.; Mueller, S. Sequential Support: 3D Printing Dissolvable Support Material for Time-Dependent Mechanisms. In *TEI 2019 - Proceedings of the 13th International Conference on Tangible, Embedded, and Embodied Interaction*; Association for Computing Machinery, Inc.: 2019; pp 669−676; DOI: 10.1145/3294109.3295630.
(38) Kumbhar, N. N.; Mulay, A. v. Post Processing Methods Used to Improve Surface Finish of Products Which Are Manufactured by Additive Manufacturing Technologies: A Review. *Journal of The Institution of Engineers (India): Series C* **2018**, *99* (4), 481−487.

(39) Boschetto, A.; Bottini, L.; Veniali, F. Finishing of Fused Deposition Modeling Parts by CNC Machining. *Robot Comput. Integr Manuf* **2016**, *41*, 92−101.
(40) Mazlan, S. N. H.; Alkahari, M. R.; Ramli, F. R.; Maidin, N. A.; Sudin, M. N.; Zolkaply, A. R. Surface Finish and Mechanical Properties of FDM Part After Blow Cold Vapor Treatment. *J. Adv. Res. Fluid Mech. Therm. Sci.* **2018**, *48*, 148−155.
(41) Moradi, M.; Karami Moghadam, M.; Shamsborhan, M.; Bodaghi, M.; Falavandi, H. Post-Processing of FDM 3D-Printed Polylactic Acid Parts by Laser Beam Cutting. *Polymers* **2020**, *12* (3), 550.
(42) Kumbhar, N. N.; Mulay, A. v. Post Processing Methods Used to Improve Surface Finish of Products Which Are Manufactured by Additive Manufacturing Technologies: A Review. *J. Inst. Eng. India Ser. C* **2018**, *99* (4), 481−487.
(43) Singamneni, S.; Roychoudhury, A.; Diegel, O.; Huang, B. Modeling and Evaluation of Curved Layer Fused Deposition. *J. Mater. Process Technol.* **2012**, *212* (1), 27−35.
(44) Chakraborty, D.; Aneesh Reddy, B.; Roy Choudhury, A. Extruder Path Generation for Curved Layer Fused Deposition Modeling. *Computer-Aided Design* **2008**, *40* (2), 235−243.
(45) Allen, R. J. A.; Trask, R. S. An Experimental Demonstration of Effective Curved Layer Fused Filament Fabrication Utilising a Parallel Deposition Robot. *Addit Manuf* **2015**, *8*, 78−87.
(46) Chen, L.; Chung, M. F.; Tian, Y.; Joneja, A.; Tang, K. Variable-Depth Curved Layer Fused Deposition Modeling of Thin-Shells. *Robot Comput. Integr Manuf* **2019**, *57*, 422−434.
(47) Mwema, F. M.; Akinlabi, E. T. Basics of Fused Deposition Modelling (FDM). *In SpringerBriefs in Applied Sciences and Technology; Springer* **2020**, 1−15.
(48) Doshi, M.; Mahale, A.; Kumar Singh, S.; Deshmukh, S. Printing Parameters and Materials Affecting Mechanical Properties of FDM-3D Printed Parts: Perspective and Prospects. *Mater. Today: Proc.* **2022**, *50*, 2269−2275.
(49) Samykano, M.; Selvamani, S. K.; Kadirgama, K.; Ngui, W. K.; Kanagaraj, G.; Sudhakar, K. Mechanical Property of FDM Printed ABS: Influence of Printing Parameters. *International Journal of Advanced Manufacturing Technology* **2019**, *102* (9−12), 2779−2796.
(50) Spoerk, M.; Gonzalez-Gutierrez, J.; Sapkota, J.; Schuschnigg, S.; Holzer, C. Effect of the Printing Bed Temperature on the Adhesion of Parts Produced by Fused Filament Fabrication. *Plastics, Rubber and Composites* **2018**, *47* (1), 17−24.
(51) Choi, Y.-H.; Kim, C.-M.; Jeong, H.-S.; Youn, J.-H. Influence of Bed Temperature on Heat Shrinkage Shape Error in FDM Additive Manufacturing of the ABS-Engineering Plastic. *World Journal of Engineering and Technology* **2016**, *04* (03), 186−192.
(52) Spoerk, M.; Gonzalez-Gutierrez, J.; Sapkota, J.; Schuschnigg, S.; Holzer, C. *Effect of the Printing Bed Temperature on the Adhesion of Parts Produced by Fused Filament Fabrication* **2018**, *47* (1), 17−24.
(53) Dey, A.; Yodo, N. A Systematic Survey of FDM Process Parameter Optimization and Their Influence on Part Characteristics. *J. Manuf. Mater. Process.* **2019**, *3*, 64.
(54) Ramanath, H. S.; Chua, C. K.; Leong, K. F.; Shah, K. D. Melt Flow Behaviour of Poly-ε-Caprolactone in Fused Deposition Modelling. *J. Mater. Sci.: Mater. Med.* **2008**, *19* (7), 2541−2550.
(55) Ansari, A. A.; Kamil, M. Effect of Print Speed and Extrusion Temperature on Properties of 3D Printed PLA Using Fused Deposition Modeling Process. *Mater. Today Proc.* **2021**, *45*, 5462−5468.
(56) Narayana, S.; Venkatesh, B. Experimental Investigation and Optimization of the Fused Deposition Modelled Acrylonitrile Butadiene Styrene. In *AIP Conference Proceedings*; AIP Publishing: 2019; 020055;
(57) Ganeshkumar, S.; Kumar, S. D.; Magarajan, U.; Rajkumar, S.; Arulmurugan, B.; Sharma, S.; Li, C.; Ilyas, R. A.; Badran, M. F. Investigation of Tensile Properties of Different Infill Pattern Structures of 3D-Printed PLA Polymers: Analysis and Validation Using Finite Element Analysis in ANSYS. *Materials* **2022**, *15* (15), 5142.
(58) Miazio, Ł. Impact of Print Speed on Strength of Samples Printed in FDM Technology. *Agricultural Engineering* **2019**, *23* (2), 33−38.
(59) Gunaydin, K.; Türkmen, H. S. Common FDM 3D Printing Defects. In *International Congress on 3D Printing (Additive Manufacturing) Technologies and Digital Industry Conference proceedings*, Antalya, Turkey, April 19−21, 2018.
(60) Yan, L.; Sun, H.; Qu, X.; Zhou, W. The Fused Deposition Modeling 3D Printing. In *International Conference on Electrical, Mechanical and Industrial Engineering proceedings*, 2016; DOI: 10.2991/icemie-16.2016.50.
(61) Wu, W.; Geng, P.; Li, G.; Zhao, D.; Zhang, H.; Zhao, J. Influence of Layer Thickness and Raster Angle on the Mechanical Properties of 3D-Printed PEEK and a Comparative Mechanical Study between PEEK and ABS. *Materials* **2015**, *8* (9), 5834−5846.
(62) Ayatollahi, M. R.; Nabavi-Kivi, A.; Bahrami, B.; Yazid Yahya, M.; Khosravani, M. R. The Influence of In-Plane Raster Angle on Tensile and Fracture Strengths of 3D-Printed PLA Specimens. *Eng. Fract. Mech.* **2020**, *237*, 107225.
(63) de Toro, E. V.; Sobrino, J. C.; Martínez, A. M.; Eguía, V. M. Analysis of the Influence of the Variables of the Fused Deposition Modeling (FDM) Process on the Mechanical Properties of a Carbon Fiber-Reinforced Polyamide. *Procedia Manuf* **2019**, *41*, 731−738.
(64) Nugroho, A.; Ardiansyah, R.; Rusita, L.; Larasati, I. L. Effect of Layer Thickness on Flexural Properties of PLA (PolyLactid Acid) by 3D Printing. In *Journal of Physics: Conference Series*; Institute of Physics Publishing: 2018; Vol. *1130*; DOI: 10.1088/1742-6596/1130/1/012017.
(65) Tsouknidas, A.; Pantazopoulos, M.; Katsoulis, I.; Fasnakis, D.; Maropoulos, S.; Michailidis, N. Impact Absorption Capacity of 3D-Printed Components Fabricated by Fused Deposition Modelling. *Mater. Des* **2016**, *102*, 41−44.
(66) Rismalia, M.; Hidajat, S. C.; Permana, I. G. R.; Hadisujoto, B.; Muslimin, M.; Triawan, F. Infill Pattern and Density Effects on the Tensile Properties of 3D Printed PLA Material. *J. Phys.: Conf. Ser.* **2019**, *1402*, 044041.
(67) Mishra, P. K.; Senthil, P.; Adarsh, S.; Anoop, M. S. An Investigation to Study the Combined Effect of Different Infill Pattern and Infill Density on the Impact Strength of 3D Printed Polylactic Acid Parts. *Compos. Commun.* **2021**, *24*, 100605.
(68) Hohimer, C.; Christ, J.; Aliheidari, N.; Mo, C.; Ameli, A. 3D Printed Thermoplastic Polyurethane with Isotropic Material Properties. In *Behavior and Mechanics of Multifunctional Materials and Composites 2017*; SPIE: 2017; Vol. *10165*, p 1016511; DOI: 10.1117/12.2259810.
(69) Özen, A.; Abali, B. E.; Völlmecke, C.; Gerstel, J.; Auhl, D. Exploring the Role of Manufacturing Parameters on Microstructure and Mechanical Properties in Fused Deposition Modeling (FDM) Using PETG. *Applied Composite Materials* **2021**, *28* (6), 1799−1828.
(70) Benwood, C.; Anstey, A.; Andrzejewski, J.; Misra, M.; Mohanty, A. K. Improving the Impact Strength and Heat Resistance of 3D Printed Models: Structure, Property, and Processing Correlationships during Fused Deposition Modeling (FDM) of Poly(Lactic Acid). *ACS Omega* **2018**, *3* (4), 4400−4411.
(71) Liparoti, S.; Sofia, D.; Romano, A.; Marra, F.; Pantani, R. Fused Filament Deposition of PLA: The Role of Interlayer Adhesion in the Mechanical Performances. *Polymers* **2021**, *13* (3), 399.
(72) Khosravani, M. R.; Berto, F.; Ayatollahi, M. R.; Reinicke, T. Characterization of 3D-Printed PLA Parts with Different Raster Orientations and Printing Speeds. *Sci. Rep.* **2022**, *12* (1), 1016.
(73) Gao, S.; Liu, R.; Xin, H.; Liang, H.; Wang, Y.; Jia, J. The Surface Characteristics, Microstructure and Mechanical Properties of PEEK Printed by Fused Deposition Modeling with Different Raster Angles. *Polymers* **2022**, *14* (1), 77.
(74) Naveed, N. Investigating the Material Properties and Microstructural Changes of Fused Filament Fabricated PLA and Tough-PLA Parts. *Polymers (Basel)* **2021**, *13* (9), 1487.
(75) Naveed, N. Investigate the Effects of Process Parameters on Material Properties and Microstructural Changes of 3D-Printed

Specimens Using Fused Deposition Modelling (FDM). *Materials Technology* **2021**, *36* (5), 317−330.
(76) Abdullah Aloyaydi, B.; Sivasankaran, S.; Rizk Ammar, H. Influence of Infill Density on Microstructure and Flexural Behavior of 3D Printed PLA Thermoplastic Parts Processed by Fusion Deposition Modeling. *AIMS Mater. Sci.* **2019**, *6* (6), 1033−1048.
(77) Ouhsti, M.; El Haddadi, B.; Belhouideg, S. Effect of Printing Parameters on the Mechanical Properties of Parts Fabricated with Open-Source 3D Printers in PLA by Fused Deposition Modeling. *Mechanics and Mechanical Engineering* **2018**, *22* (4), 895−908.
(78) Kaveh, M.; Badrossamay, M.; Foroozmehr, E.; Hemasian Etefagh, A. Optimization of the Printing Parameters Affecting Dimensional Accuracy and Internal Cavity for HIPS Material Used in Fused Deposition Modeling Processes. *J. Mater. Process Technol.* **2015**, *226*, 280−286.
(79) Wang, P.; Zou, B.; Ding, S.; Li, L.; Huang, C. Effects of FDM-3D Printing Parameters on Mechanical Properties and Microstructure of CF/PEEK and GF/PEEK. *Chinese Journal of Aeronautics* **2021**, *34* (9), 236−246.
(80) Patanwala, H. S.; Hong, D.; Vora, S. R.; Bognet, B.; Ma, A. W. K. The Microstructure and Mechanical Properties of 3D Printed Carbon Nanotube-Polylactic Acid Composites. *Polym. Compos.* **2018**, *39*, E1060−E1071.
(81) Khan, A.; Khan, A. A. P.; Asiri, A. M.; Alamry, K. A. Preparation and Characterization of Hybrid Graphene Oxide Composite and Its Application in Paracetamol Microbiosensor. *Polym. Compos* **2015**, *36* (2), 221−228.
(82) Ansari, M. A. A.; Golebiowska, A. A.; Dash, M.; Kumar, P.; Jain, P. K.; Nukavarapu, S. P.; Ramakrishna, S.; Nanda, H. S. Engineering Biomaterials to 3D-Print Scaffolds for Bone Regeneration: Practical and Theoretical Consideration. *Biomater Sci.* **2022**, *10* (11), 2789−2816.
(83) Lavecchia, F.; Guerra, M. G.; Galantucci, L. M. Chemical Vapor Treatment to Improve Surface Finish of 3D Printed Polylactic Acid (PLA) Parts Realized by Fused Filament Fabrication. *Prog. Addit. Manuf.* **2022**, *7* (1), 65−75.
(84) Chohan, J. S.; Singh, R.; Boparai, K. S. Vapor Smoothing Process for Surface Finishing of FDM Replicas. *Mater. Today Proc.* **2020**, *26*, 173−179.
(85) Neff, C.; Trapuzzano, M.; Crane, N. B. Impact of Vapor Polishing on Surface Roughness and Mechanical Properties for 3D Printed ABS. https://hdl.handle.net/2152/89775 (accessed 2023-01-25).
(86) Kosorn, W.; Sakulsumbat, M.; Uppanan, P.; Kaewkong, P.; Chantaweroad, S.; Jitsaard, J.; Sitthiseripratip, K.; Janvikul, W. PCL/PHBV Blended Three Dimensional Scaffolds Fabricated by Fused Deposition Modeling and Responses of Chondrocytes to the Scaffolds. *J. Biomed. Mater. Res.* **2017**, *105* (5), 1141−1150.
(87) Ansari, V.; Calore, A.; Zonderland, J.; Harings, J. A. W.; Moroni, L.; Bernaerts, K. v. Additive Manufacturing of α-Amino Acid Based Poly(Ester Amide)s for Biomedical Applications. *Biomacromolecules* **2022**, *23* (3), 1083−1100.
(88) Lerman, M. J.; Muramoto, S.; Arumugasaamy, N.; van Order, M.; Lembong, J.; Gerald, A. G.; Gillen, G.; Fisher, J. P. Development of Surface Functionalization Strategies for 3D-Printed Polystyrene Constructs. *J. Biomed Mater. Res. B Appl. Biomater* **2019**, *107* (8), 2566−2578.
(89) Richbourg, N. R.; Peppas, N. A.; Sikavitsas, V. I. Tuning the Biomimetic Behavior of Scaffolds for Regenerative Medicine through Surface Modifications. *J. Tissue Eng. Regen Med.* **2019**, *13* (8), 1275−1293.
(90) Donate, R.; Alemán-Domínguez, M. E.; Monzón, M. On the Effectiveness of Oxygen Plasma and Alkali Surface Treatments to Modify the Properties of Polylactic Acid Scaffolds. *Polymers* **2021**, *13* (10), 1643.
(91) Song, Y.; Ren, M.; Wu, Y.; Li, S.; Song, C.; Wang, F.; Huang, Y. The Effect of Different Surface Treatment Methods on the Physical, Chemical and Biological Performances of a PGA Scaffold. *RSC Adv.* **2019**, *9* (35), 20174−20184.
(92) Iturriaga, L.; Van Gordon, K. D.; Larrañaga-Jaurrieta, G.; Camarero-Espinosa, S. Strategies to Introduce Topographical and Structural Cues in 3D-Printed Scaffolds and Implications in Tissue Regeneration. *Adv. Nanobiomed. Res.* **2021**, *1* (12), 2100068.
(93) Griffin, M.; Palgrave, R.; Baldovino-Medrano, V. G.; Butler, P. E.; Kalaskar, D. M. Argon Plasma Improves the Tissue Integration and Angiogenesis of Subcutaneous Implants by Modifying Surface Chemistry and Topography. *Int. J. Nanomedicine* **2018**, *13*, 6123−6141.
(94) Asadian, M.; Dhaenens, M.; Onyshchenko, I.; de Waele, S.; Declercq, H.; Cools, P.; Devreese, B.; Deforce, D.; Morent, R.; de Geyter, N. Plasma Functionalization of Polycaprolactone Nanofibers Changes Protein Interactions with Cells, Resulting in Increased Cell Viability. *ACS Appl. Mater. Interfaces* **2018**, *10* (49), 41962−41977.
(95) Popelka, A.; Novák, I.; Al-Maadeed, M. A. S. A.; Ouederni, M.; Krupa, I. Effect of Corona Treatment on Adhesion Enhancement of LLDPE. *Surf. Coat. Technol.* **2018**, *335*, 118−125.
(96) Girão, A. F.; Wieringa, P.; Pinto, S. C.; Marques, P. A. A. P.; Micera, S.; van Wezel, R.; Ahmed, M.; Truckenmueller, R.; Moroni, L. Ultraviolet Functionalization of Electrospun Scaffolds to Activate Fibrous Runways for Targeting Cell Adhesion. *Front. Bioeng. Biotechnol.* **2019**, *7*, 159.
(97) Sutherland, I.; Brewis, D. M.; Health, R. J.; Sheng, E. Modification of Polypropylene Surfaces by Flame Treatment. *Surf. Interface Anal.* **1991**, *17* (7), 507−510.
(98) Amin Yavari, S.; Croes, M.; Akhavan, B.; Jahanmard, F.; Eigenhuis, C. C.; Dadbakhsh, S.; Vogely, H. C.; Bilek, M. M.; Fluit, A. C.; Boel, C. H. E.; van der Wal, B. C. H.; Vermonden, T.; Weinans, H.; Zadpoor, A. A. Layer by Layer Coating for Bio-Functionalization of Additively Manufactured Meta-Biomaterials. *Addit Manuf* **2020**, *32*, 100991.
(99) Jose, J.; Sultan, S.; Kalarikkal, N.; Thomas, S.; Mathew, A. P. Fabrication and Functionalization of 3D-Printed Soft and Hard Scaffolds with Growth Factors for Enhanced Bioactivity. *RSC Adv.* **2020**, *10* (62), 37928−37937.
(100) Liu, J.; Mohd Rafiq, N. B.; Wong, L. M.; Wang, S. Surface Treatment and Bioinspired Coating for 3D-Printed Implants. *Front. Chem.* **2021**, *9*, 768007.
(101) Petitjean, L.; Reffay, M.; Grasland-Mongrain, E.; Poujade, M.; Ladoux, B.; Buguin, A.; Silberzan, P. Velocity Fields in a Collectively Migrating Epithelium. *Biophys. J.* **2010**, *98* (9), 1790−1800.
(102) Chen, S.; Shi, Y.; Luo, Y.; Ma, J. Layer-by-Layer Coated Porous 3D Printed Hydroxyapatite Composite Scaffolds for Controlled Drug Delivery. *Colloids Surf. B Biointerfaces* **2019**, *179*, 121−127.
(103) de Villiers, M. M.; Otto, D. P.; Strydom, S. J.; Lvov, Y. M. Introduction to Nanocoatings Produced by Layer-by-Layer (LbL) Self-Assembly. *Adv. Drug Deliv Rev.* **2011**, *63* (9), 701−715.
(104) Keeney, M.; Jiang, X. Y.; Yamane, M.; Lee, M.; Goodman, S.; Yang, F. Nanocoating for Biomolecule Delivery Using Layer-by-Layer Self-Assembly. *J. Mater. Chem. B* **2015**, *3* (45), 8757−8770.
(105) Zhang, S.; Xing, M.; Li, B. Biomimetic Layer-by-Layer Self-Assembly of Nanofilms, Nanocoatings, and 3D Scaffolds for Tissue Engineering. *Int. J. Mol. Sci.* **2018**, *19* (6), 1641.
(106) Kubies, D.; Machová, L.; Brynda, E.; Lukáš, J.; Rypáček, F. Functionalized Surfaces of Polylactide Modified by Langmuir-Blodgett Films of Amphiphilic Block Copolymers. *J. Mater. Sci. Mater. Med.* **2003**, *14* (2), 143−149.
(107) de Souza, I. D.; Cruz, M. A. E.; de Faria, A. N.; Zancanela, D. C.; Simão, A. M. S.; Ciancaglini, P.; Ramos, A. P. Formation of Carbonated Hydroxyapatite Films on Metallic Surfaces Using Dihexadecyl Phosphate-LB Film as Template. *Colloids Surf. B Biointerfaces* **2014**, *118*, 31−40.
(108) Datta, P.; Ayan, B.; Ozbolat, I. T. Bioprinting for Vascular and Vascularized Tissue Biofabrication. *Acta Biomater* **2017**, *51*, 1−20.
(109) Kubies, D.; Machová, L.; Brynda, E.; Lukáš, J.; Rypáček, F. Functionalized Surfaces of Polylactide Modified by Langmuir-Blodgett Films of Amphiphilic Block Copolymers. *J. Mater. Sci. Mater. Med.* **2003**, *14* (2), 143−149.

https://doi.org/10.1021/acsomega.2c05984
ACS Omega 2023, 8, 5139−5156

(110) Schöne, A. C.; Roch, T.; Schulz, B.; Lendlein, A. Evaluating Polymeric Biomaterial-Environment Interfaces by Langmuir Monolayer Techniques. *J. R. Soc. Interface* **2017**, *14* (130), 20161028.
(111) Calejo, M. T.; Ilmarinen, T.; Vuorimaa-Laukkanen, E.; Talvitie, E.; Hakola, H. M.; Skottman, H.; Kellomäki, M. Langmuir-Schaefer Film Deposition onto Honeycomb Porous Films for Retinal Tissue Engineering. *Acta Biomater* **2017**, *54*, 138−149.
(112) Shuai, C.; Yang, Y.; Feng, P.; Peng, S.; Guo, W.; Min, A.; Gao, C. A Multi-Scale Porous Scaffold Fabricated by a Combined Additive Manufacturing and Chemical Etching Process for Bone Tissue Engineering. *Int. J. Bioprint.* **2018**, *4* (2), 133.
(113) Paragkumar N, T.; Edith, D.; Six, J. L. Surface Characteristics of PLA and PLGA Films. *Appl. Surf. Sci.* **2006**, *253* (5), 2758−2764.
(114) Baran, E. H.; Erbil, H. Y. Surface Modification of 3D Printed PLA Objects by Fused Deposition Modeling: A Review. *Colloids Interfaces* **2019**, *3* (2), 43.
(115) Lerman, M. J.; Muramoto, S.; Arumugasaamy, N.; van Order, M.; Lembong, J.; Gerald, A. G.; Gillen, G.; Fisher, J. P. Development of Surface Functionalization Strategies for 3D-Printed Polystyrene Constructs. *J. Biomed Mater. Res. B Appl. Biomater* **2019**, *107* (8), 2566−2578.
(116) Guo, C.; Xiang, M.; Dong, Y. Surface Modification of Poly (Lactic Acid) with an Improved Alkali-Acid Hydrolysis Method. *Mater. Lett.* **2015**, *140*, 144−147.
(117) Meng, B.; Wang, X. H.; Cui, F. Z.; Dong, H. Y.; Yu, F. *A New Method of Heparinizing PLLA Film by Surface Entrapment* **2004**, *19* (2), 131−143.
(118) Jaidev, L. R.; Chatterjee, K. Surface Functionalization of 3D Printed Polymer Scaffolds to Augment Stem Cell Response. *Materials & Design* **2019**, *161*, 44−54.
(119) Lerman, M. J.; Muramoto, S.; Arumugasaamy, N.; van Order, M.; Lembong, J.; Gerald, A. G.; Gillen, G.; Fisher, J. P. Development of Surface Functionalization Strategies for 3D-Printed Polystyrene Constructs. *J. Biomed Mater. Res. B Appl. Biomater* **2019**, *107* (8), 2566−2578.
(120) Edlund, U.; Källrot, M.; Albertsson, A. C. Single-Step Covalent Functionalization of Polylactide Surfaces. *J. Am. Chem. Soc.* **2005**, *127* (24), 8865−8871.
(121) Janorkar, A. v.; Metters, A. T.; Hirt, D. E. Modification of Poly(Lactic Acid) Films: Enhanced Wettability from Surface-Confined Photografting and Increased Degradation Rate Due to an Artifact of the Photografting Process. *Macromolecules* **2004**, *37* (24), 9151−9159.
(122) Liu, J.; Mohd Rafiq, N. B.; Wong, L. M.; Wang, S. Surface Treatment and Bioinspired Coating for 3D-Printed Implants. *Front Chem.* **2021**, *9*, 768007.
(123) Zhang, B. G. X.; Myers, D. E.; Wallace, G. G.; Brandt, M.; Choong, P. F. M. Bioactive Coatings for Orthopaedic Implants-Recent Trends in Development of Implant Coatings. *Int. J. Mol. Sci.* **2014**, *15* (7), 11878−11921.
(124) Zhang, B.; Wang, L.; Song, P.; Pei, X.; Sun, H.; Wu, L.; Zhou, C.; Wang, K.; Fan, Y.; Zhang, X. 3D Printed Bone Tissue Regenerative PLA/HA Scaffolds with Comprehensive Performance Optimizations. *Mater. Des* **2021**, *201*, 109490.
(125) Kalova, M.; Rusnakova, S.; Krzikalla, D.; Mesicek, J.; Tomasek, R.; Podeprelova, A.; Rosicky, J.; Pagac, M. 3D Printed Hollow Off-Axis Profiles Based on Carbon Fiber-Reinforced Polymers: Mechanical Testing and Finite Element Method Analysis. *Polymers* **2021**, *13* (17), 2949.
(126) Lim, T.; Cheng, H.; Song, W.; Lee, J.; Kim, S.; Jung, W. Simulated and Experimental Investigation of Mechanical Properties for Improving Isotropic Fracture Strength of 3D-Printed Capsules. *Materials (Basel)* **2021**, *14* (16), 4677.
(127) Lepoivre, A.; Boyard, N.; Levy, A.; Sobotka, V. Heat Transfer and Adhesion Study for the FFF Additive Manufacturing Process. *Procedia Manuf* **2020**, *47*, 948−955.
(128) Zhang, M.; Li, Y.; Kolluru, P. v.; Brinson, L. C. Determination of Mechanical Properties of Polymer Interphase Using Combined Atomic Force Microscope (AFM) Experiments and Finite Element Simulations. *Macromolecules* **2018**, *51* (20), 8229−8240.
(129) Ramanath, H. S.; Chua, C. K.; Leong, K. F.; Shah, K. D. Melt Flow Behaviour of Poly-Epsilon-Caprolactone in Fused Deposition Modelling. *J. Mater. Sci. Mater. Med.* **2008**, *19* (7), 2541−2550.
(130) Nasirov, A.; Fidan, I. Prediction of Mechanical Properties of Fused Filament Fabricated Structures via Asymptotic Homogenization. *Mechanics of Materials* **2020**, *145*, 103372.
(131) Ferreira, R. T. L.; Amatte, I. C.; Dutra, T. A.; Bürger, D. Experimental Characterization and Micrography of 3D Printed PLA and PLA Reinforced with Short Carbon Fibers. *Compos B Eng.* **2017**, *124*, 88−100.
(132) Qin, X.; Wu, Y.; Liu, S.; Yang, L.; Yuan, H.; Cai, S.; Flesch, J.; Li, Z.; Tang, Y.; Li, X.; Zhuang, Y.; You, C.; Liu, C.; Yu, C. Surface Modification of Polycaprolactone Scaffold With Improved Biocompatibility and Controlled Growth Factor Release for Enhanced Stem Cell Differentiation. *Front. Bioeng. Biotechnol.* **2022**, *9*, 802311.
(133) Do, A. V.; Smith, R.; Acri, T. M.; Geary, S. M.; Salem, A. K. 3D Printing Technologies for 3D Scaffold Engineering. *Functional 3D Tissue Engineering Scaffolds: Materials, Technologies, and Applications* **2018**, 203−234.
(134) Qi, S.; Fu, J.; Xie, Y.; Li, Y.; Gan, R.; Yu, M. Versatile Magnetorheological Plastomer with 3D Printability, Switchable Mechanics, Shape Memory, and Self-Healing Capacity. *Compos. Sci. Technol.* **2019**, *183*, 107817.
(135) Neufurth, M.; Wang, X.; Wang, S.; Steffen, R.; Ackermann, M.; Haep, N. D.; Schröder, H. C.; Müller, W. E. G. 3D Printing of Hybrid Biomaterials for Bone Tissue Engineering: Calcium-Polyphosphate Microparticles Encapsulated by Polycaprolactone. *Acta Biomater* **2017**, *64*, 377−388.
(136) Kim, K.; Lee, C. H.; Kim, B. K.; Mao, J. J. Anatomically Shaped Tooth and Periodontal Regeneration by Cell Homing. *J. Dent Res.* **2010**, *89* (8), 842−847.
(137) Li, J.; Chen, M.; Wei, X.; Hao, Y.; Wang, J. Evaluation of 3D-Printed Polycaprolactone Scaffolds Coated with Freeze-Dried Platelet-Rich Plasma for Bone Regeneration. *Materials (Basel)* **2017**, *10* (7), 831.
(138) Narita, M.; Takaki, T.; Shibahara, T.; Iwamoto, M.; Yakushiji, T.; Kamio, T. Utilization of Desktop 3D Printer-Fabricated "Cost-Effective" 3D Models in Orthognathic Surgery. *Maxillofacial Plastic and Reconstructive Surgery 2020 42:1* **2020**, *42* (1), 1−7.
(139) Zhou, Y.; Grayson, W. Three-Dimensional Printing of Scaffolds for Facial Reconstruction. *MRS Bull.* **2022**, *47*, 91−97.
(140) He, D.; Liang, J.; Wang, H.; Jiao, Y.; Wu, B.; Cui, D.; Cao, T.; Li, Y.; Wang, J.; Zhang, B. 3D-Printed PEEK Extravascular Stent in the Treatment of Nutcracker Syndrome: Imaging Evaluation and Short-Term Clinical Outcome. *Front. Bioeng. Biotechnol.* **2020**, *8*, 732.

https://doi.org/10.1021/acsomega.2c05984
ACS Omega 2023, 8, 5139−5156